Investigation of high-temperature stability of AlN, sapphire and their hetero-interface for heteroepitaxy

Kazuya Takada

Department of Applied Chemistry
Graduate School of Engineering
Tokyo University of Agriculture and Technology

2018

Contents

Chapter 1 Introduction

It is expected that aluminum nitride (AlN) will be applied to fabrication of deep-UV light emitting diodes because its bandgap energy is the widest of any direct transition semiconductor materials [1-14]. Power devices are also promising applications of AlN thanks to its unique features such as high thermal conductivity and high breakdown field [15-17]. In order to manufacture these devices, high quality single crystalline AlN substrates/templates are crucial as base substrates on which device structures are fabricated.

Many reports have been published on preparation of low-dislocation density bulk AlN crystals by physical vapor transport (PVT) [18-25]. However, PVT method, by its nature, is difficult to avoid incorporation of impurities such as carbon and oxygen, leading to degradation of optical transmittance in deep-UV region [22-24]. On the other hand, hydride vapor phase epitaxy (HVPE) can grow high-purity AlN at a high rate, although crystals grown contain high density of dislocations in the case of heteroepitaxy [26-32]. Our group has recently demonstrated preparation of low dislocation density and deep-UV transparent freestanding AlN substrates by HVPE using PVT-AlN starting substrates [33, 34].

However, it is still worth trying to grow thick AlN layers with low dislocation density on sapphire substrates by HVPE, which is followed by separation at the interface. If the heteroepitaxial growth technique can be realized, the industry will receive significant economic benefits of the immediate availability of low-cost sapphire substrates up to 8 inches in diameter.

Our group already reported rapid growth (85 μm/h) of an AlN epitaxial layer on a (0001) sapphire substrate at 1380 °C by HVPE [35]. Although the crystalline quality

of AlN layers can be improved by growing at temperatures over 1200 °C, the thermal stability and/or decomposition of AlN at such high temperatures have yet to be investigated. Understanding these issues is particularly important for using AlN templates or substrates at high temperatures. In addition, because the net growth rate of AlN is given by the deposition rate minus the decomposition rate, an increase in the AlN decomposition rate might decrease the net growth rate of AlN at high temperatures. There are also two possible polarities for the (0001) AlN surface, i.e., Al- and N-polarity. Thus, the polarity dependence of the AlN decomposition rate is another important issue that needs to be clarified in order to identify the most stable polarity at high temperatures and the mechanisms for developing one of the polarities while AlN grows.

In Chapter 2 of this thesis, the thermal stabilities and decomposition of Al- and N-polarity AlN layers which are grown on (0001) sapphire substrates are investigated in the temperature ranging from 1100 to 1400 °C and in various gas flows (He, H_2 and H_2+NH_3). The difference in the AlN decomposition rates between Al- and N-polarity AlN surfaces is discussed in relation to surface bonding structure of AlN.

In Chapter 3 of this thesis, the effect of heat treatment on (0001) sapphire substrates is examined in the temperature which ranges from 980 to 1480 °C for an atmospheric-pressure mixed flow of H_2 and N_2 with various molar fractions of H_2. Only when N_2 coexists with H_2 in the temperature range of 1030–1430 °C undesirable whiskers of AlN form on the sapphire surface. The decomposition of the sapphire substrate and the formation of AlN on the sapphire surface are also investigated by thermodynamic analysis.

In Chapter 4 of this thesis, the formation mechanism of the undesirable AlN whiskers on (0001) sapphire substrates reported in the preceding chapter is investigated in the

temperature range of 980–1380 °C and in an atmospheric-pressure mixed flow of H_2 and N_2 with $F°$ [= H_2 / (H_2 + N_2)] of 0.750 (H_2/N_2 = 3/1).

After successfully demonstrating HVPE of AlN using $AlCl_3$ and NH_3 as source gases [36], our group has been investigating the growth of thick and high quality AlN layers on (0001) sapphire at temperatures above 1200 °C [35, 37-39]. However, the high growth temperature induces a greater mismatch of thermal expansion between the AlN grown layer and the sapphire substrate during post-growth cooling to room temperature (RT), which results in cracking of both the AlN layer and the sapphire substrate.

In order to overcome the thermal expansion mismatch, *in situ* self-separation of thick GaN layers at high temperatures by void assisted separation was reported for successful production of freestanding GaN substrates by HVPE using sapphire starting substrates [40]. In an attempt to develop a similar method for the *in situ* self-separation of thick AlN layers from sapphire substrates at high temperatures, in Chapter 5 of this thesis, the mechanism of void formation at the interface is investigated for the reproducible self-separation of thick and large area AlN layers from sapphire substrates with the assistance of voids as a predefined separation point. In addition, the properties of the self-separated freestanding AlN substrates are investigated.

Chapter 2 Polarity dependence of AlN {0001} decomposition in flowing H_2

2.1. Experimental procedure

First, two kinds of AlN layers, which are Al- and N-polarity layers, were grown on 2-inch-diameter (0001) sapphire substrates by MOVPE (AIXTRON AIX200/4 RF-S) where trimethylaluminum (TMA) and NH_3 as source gases and H_2 as a carrier gas were utilized. The Al-polarity AlN layer was grown at 1300 ºC by growing 17-nm-thick seed AlN layer first by simultaneous supply of TMA and NH_3 and subsequently growing the main AlN layer by alternating supply of TMA and NH_3. The growth process is described in detail elsewhere [41]. The N-polarity AlN layer was grown via surface nitridation of the sapphire substrate at 620 ºC, by growing a 5.2-nm-thick low-temperature (LT)-AlN buffer layer at 620 ºC by simultaneously supplying TMA and NH_3, and then growing the main AlN layer at 1270 ºC by supplying TMA and NH_3 alternatingly. Experimental details can be found elsewhere [41].

Specimens (5 mm × 5 mm) for high temperature heating experiments were cut from the above-mentioned 2-inch-diameter sapphire substrates with the AlN layers. Before the initiation of the heating experiments, the initial thickness, crystalline quality and polarity of the AlN layers were determined by scanning electron microscopy (SEM) (JEOL, JSM-6700F), X-ray diffraction (XRD) (Spectris, X'Pert PRO MRD) and wet chemical etching in potassium hydroxide (KOH) solution [42], respectively. There was no change in thickness and surface morphology on wet chemical etching of the Al-polarity AlN layer, which indicates that no N-polarity inversion domains (IDs) in the Al-polarity grown layer

existed. By contrast, almost the entire N-polarity AlN layer was etched away by the KOH solution, although a small number of hexagonal pyramids defined by $\{10\bar{1}1\}$ facets remained on the surface. These hexagonal pyramids are Al-polarity IDs contained in the N-polarity AlN matrix. The average height of the pyramids was nearly equal to the thickness of the initial layer, suggesting the emergence of the tips of the Al-polarity IDs in N-polarity matrix at the layer surface. The thickness, the full-widths at half-maximum (FWHMs) of the XRD rocking curves and the ID densities of the Al- and N-polarity AlN layers are listed on Table 2-1. Although the N-polarity AlN layer contained a small volume fraction of IDs, it was confirmed that the Al- and N-polarity AlN layers had almost identical crystalline quality.

The high temperature heating experiments were carried out with an image furnace consisting of a 2.5 kW halogen lamp, an ellipsoidal mirror and a quartz glass reactor. The AlN on sapphire specimens were placed on a graphite susceptor which was positioned at the focal point of the mirror. They were then heated to temperatures which ranged from 1100 to 1400 ºC. The pressure in the reactor was 1 atm, and He, H_2 or H_2 + NH_3 (the partial pressure of NH_3 was 5.0×10^{-2} atm) was flowed through the reactor at a total flow rate of 1000 standard cubic centimeters per minute (sccm). Followed by heating to a high temperature, the surface morphology and the thickness of the AlN layer were examined by SEM observation.

2.2. Results and discussion

Fig. 2-1 shows bird's-eye view SEM micrographs of N-polarity AlN layers before (Fig. 2-1(a)) and after heating at 1400 ºC for 1 h in He (Fig. 2-1(b)), H_2 (Fig. 2-1(c)) or H_2 + NH_3 (Fig. 2-1(d)) flow. It is obvious that there is no change in the surface

morphology and thickness of the AlN layer on heating in a He flow (Fig. 2-1(b)). This implies decomposition of AlN is negligible by the following chemical reaction at 1400 ºC:

$$\mathrm{AlN(s)} = \mathrm{Al(g)} + \frac{1}{2}\mathrm{N_2(g)}. \qquad (2\text{-}1)$$

On the other hand, there is a significant decrease in the thickness of the AlN layer after heating in flowing H_2 (Fig. 2-1(c)), revealing the decomposition of AlN. In addition, a small number of hexagonal pyramids with an average height that is greater than the thickness of the initial layer formed on the surface. In the case of GaN decomposition in flowing H_2, Koleske et al. reported the formation of Ga droplets on the surface [43]. However, cathodoluminescence (SEM, JEOL JSM-6380, with a grating monochromator, HORIBA MP-32M) spectra obtained from a hexagonal pyramid and the resistance of the hexagonal pyramids to hydrochloric acid revealed that it was not Al droplets but AIN pyramids defined by $\{10\bar{1}2\}$ facets that had regrown during heating. The formation mechanism of the AlN pyramids in the process of AlN decomposition is discussed later in this chapter. It was also revealed that adding NH_3 to H_2 could completely suppress the decomposition of AlN in flowing H_2. Fig. 2-1(d) shows that the surface morphology and thickness of the AlN layer after heating in $H_2 + NH_3$ flow remain the same as those before heating. Almost the same results as those described above were achieved when Al-polarity AlN specimens were utilized, except the fact that AlN pyramids formed on the surface. Thus, the use of an inert gas or $H_2 + NH_3$ gas flow is recommended when AlN layer is raised to high temperatures of about 1400 ºC. Finally, because the decomposition of AlN is promoted by H_2 but suppressed by NH_3, the decomposition reaction of AlN at high temperatures in flowing H_2 is inferred to be as follows:

$$\mathrm{AlN(s)} + \frac{x\ +\ 3}{2}\mathrm{H_2(g)} = \mathrm{AlH}_x\mathrm{(g)} + \mathrm{NH_3(g)}, \qquad (2\text{-}2)$$

where x is an integer between 0 and 3.

Next, the temperature dependence of the decomposition rates of Al- and N-polarity AlN layers in flowing H_2 were examined in the temperature which ranged from 1100 to 1400 ºC. In order to prevent the AlN layer from decomposing during the temperature ramping process, and to make sure that all the specimens had the same surface conditions just before the decomposition started, all specimens were first heated to 1400 ºC in a H_2 + NH_3 flow and kept for 1 h, and then the temperature was changed to the target temperature, and the NH_3 supply was stopped to initiate the decomposition of AlN. The influence of the surface oxide (AlO_x) on the decomposition of AlN was concerned. However, because the surface oxide is very thin, and the decomposed depth increased linearly with an increase of heating time in H_2, presence of surface oxide is negligible in this study. Fig. 2-2 shows the temperature dependences of the AlN decomposition rates for the Al- and N-polarity AlN layers in flowing H_2, with the decomposition rates of Ga- and N-polarity GaN surfaces in flowing H_2 shown for comparison, which our group measured with an in situ gravimetric monitoring system, [44]. This Figure shows that the decomposition rates of AlN and GaN increase as the heating temperature increases. However, the temperature at which the decomposition rate starts to rise sharply is about 1300 ºC for AlN, about 600 ºC higher than that for GaN (700 ºC). The decomposition rate of AlN at 1400 ºC is 0.3−0.5 μm/h, which is close to the typical growth rate of AlN by MOVPE. This suggests that the AlN growth rate by MOVPE decreases at 1400 ºC or above.

On the other hand, as shown in Fig. 2-2, the decomposition rates of the Al-polarity AlN layers are lower than those of the N-polarity AlN layers for each temperature. For

the case of GaN decomposition in flowing H_2, it has been made clear that the rate-limiting process of GaN decomposition is the formation of GaH at the surface [44]. On the basis of the analogy with GaN, it is speculated that the rate-limiting process of AlN decomposition is formation of AlH_x. It is inferred that the reason why the decomposition rate of the Al-polarity AlN surface is lower than that of the N-polarity AlN surface is because the topmost Al atoms on the Al-polarity AlN surface each has three back-bonds to N atoms, while the Al atoms on the N-polarity AlN surface each has one back-bond to only one N atom. The difference in the decomposition rates between Al- and N-polarity AlN is important because it indicates that a higher net growth rate can be expected on an Al-polarity AlN surface than on a N-polarity surface owing to the lower decomposition rate of the Al-polarity AlN surface. Furthermore, even when Al- and N-polarity domains coexist on the starting surface, Al-polarity domains may cover the N-polarity domains after a thick AlN layer has grown due to the faster growth rate on Al-polarity domains.

The observation of the surface morphology of the AlN layers after heating in flowing H_2 at various temperatures ascertain the uniformity of the decomposed AlN surfaces. Fig. 2-3 shows surface SEM micrographs of Al- and N-polarity AlN layers before and after heating at various temperatures for 1 h. The surfaces of both Al- and N-polarity AlN layers remain almost the same after heating at 1200 ºC because the decomposition of the surfaces is negligible. In the case of the Al-polarity AlN layer, it can be seen that the AlN decomposes uniformly during heating over 1300 ºC, even though a small number of pits form on the surface. The density of the surface pits in Fig. 2-3(d) is roughly 5×10^7 cm^{-2}, which is less than the total dislocation density in the layer (on the order of 10^{10} cm^{-2}) estimated from the FWHMs of the XRD rocking curves listed in Table 2-1 using the equation Gay et al. introduced [45]. Additionally, the shape of the pits is linear with three-fold rotational symmetry. The pit is thus considered to result from the faster

decomposition rate at domain boundaries in the layer. Therefore, Al-polarity AlN surface decomposition without the formation of pits should be possible if high-quality AlN is produced.

On the other hand, a small number of pyramids were formed on the N-polarity AlN surface during heating at 1400 ºC (Fig. 2-3(h)). As explained in Fig. 2-1(c), the pyramids are AlN defined by $\{10\bar{1}2\}$ facets that grown again while the surrounding AlN decomposed. The density of the AlN pyramids was 6×10^6 cm^{-2}, which is approximately the same as that of the Al-polarity IDs existing on the initial surface of the N-polarity matrix (see Table 2-1). This suggests that Al-polarity AlN IDs regrow while the N-polarity AlN matrix layer decomposes. Because the decomposition of AlN in flowing H_2 occurs by Eq. (2-2), and the decomposition rate of the Al-polarity AlN surface is lower than that of the N-polarity AlN surface, it is considered that the decomposition of N-polarity AlN matrix layer produces plenty of AlH_x and NH_3, which makes the net growth rate (the deposition rate minus the decomposition rate) positive on the Al-polarity IDs. To use N-polarity AlN surfaces at high temperatures is essential so that they do not include Al-polarity IDs.

Fig. 2-4 shows the Arrhenius plot of the decomposition rates of Al- and N-polarity AlN layers in flowing H_2. Exponential fits give activation energies of 399 and 450 kJ/mol for Al- and N-polarity AlN layers, respectively. These values are much lower than the value of 520 kJ/mol Fan et al. [46] reported, which was obtained by AlN decomposition in vacuum. This is because of the difference in the reaction process of AlN decomposition between in H_2 and in vacuum. On the other hand, the activation energies for Al- and N-polarity AlN decomposition are much higher than those for decomposition of Ga- and N-polarity GaN surfaces in flowing H_2 (242 and 259 kJ/mol, respectively) [44]. The higher activation energies for Al- and N-polarity AlN surfaces are considered to be a

consequence of the higher binding energy of the Al-N bond compared to the binding energy of the Ga-N bond because the activation energies of AlN and GaN decomposition in flowing H_2 are for the processes of AlH_x and GaH formation, respectively.

2.3. Conclusions

The thermal stabilities and decomposition of Al- and N-polarity AlN layers grown by MOVPE on (0001) sapphire substrates were investigated at temperatures which ranged from 1100 to 1400 ºC in various gas flows. It was found that substantial decomposition of AlN took place when AlN was heated in flowing H_2 at temperatures over 1200 ºC, and that the decomposition rate increased as the heating temperature rose. Decomposition of AlN layers was not observed in He or $H_2 + NH_3$ flow and the decomposition rates of Al-polarity AlN layers were lower than those of N-polarity AlN layers. This difference in the decomposition rates between Al- and N-polarity AlN layers could be explained when the rate-limiting processes and bonding structures on the AlN surfaces are taken into consideration. These results are potentially useful to produce AlN templates or substrates at high temperatures.

Figures and a table

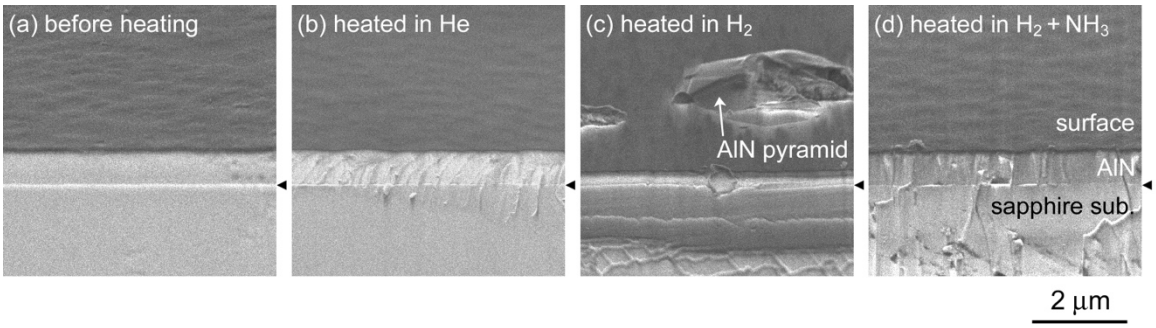

Fig. 2-1. Bird's-eye view SEM micrographs of N-polarity AlN layers (a) before heating and (b−d) after heating at 1400 ºC for 1 h in various gas flows: (b) He, (c) H_2 and (d) H_2 + NH_3. Triangular arrows indicate the interface between the AlN layer and the sapphire substrate.

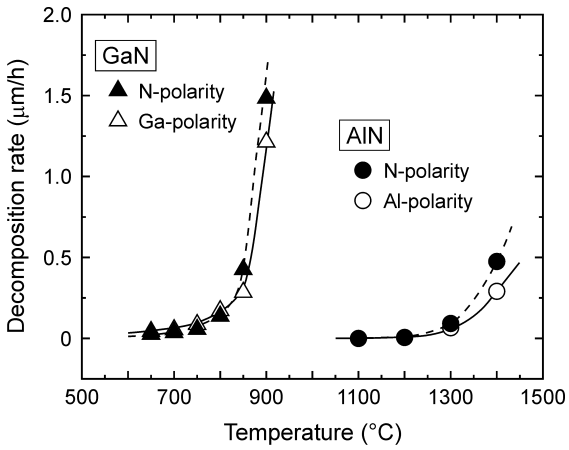

Fig. 2-2. Plot of AlN decomposition rates in flowing H_2 for various temperatures: Al-polarity AlN (open circles) and N-polarity AlN (solid circles) layers. GaN decomposition rates on Ga-polarity (open triangles) and N-polarity (solid triangles) surfaces in flowing H_2 are also plotted.

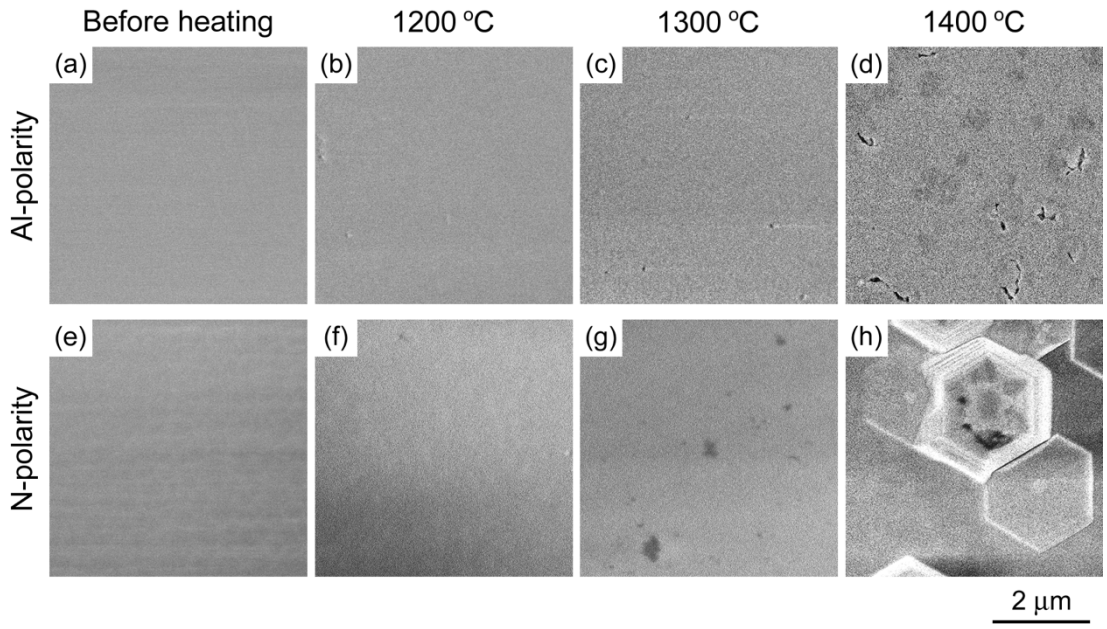

Fig. 2-3. Surface SEM micrographs of Al- and N-polarity AlN layers (a) (e) before heating and (b−d, f−h) after heating in flowing H_2 at various temperatures for 1 h: (b) (f) 1200 ºC, (c) (g) 1300 ºC and (d) (h) 1400 ºC.

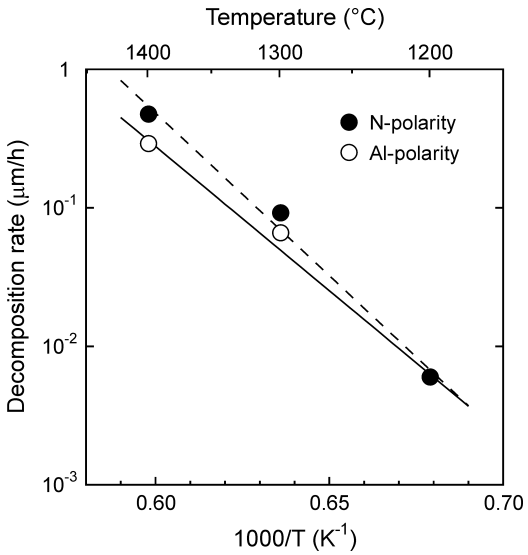

Fig. 2-4. Arrhenius plot of the AlN decomposition rates in flowing H_2: Al-polarity layer (open circles) and N-polarity layer (solid circles).

Specimen	Thickness	FWHM (arcsec)		ID density
	(μm)	(0002) plane	(10$\bar{1}$0) plane	(cm^{-2})
Al-polarity AlN	0.528	90	2167	0
N-polarity AlN	0.753	40	2160	4.6×10^6

Table 2-1. Thickness, FWHMs of XRD rocking curves for symmetric (0002) and asymmetric (10$\bar{1}$0) planes, and ID density of Al- and N-polarity AlN layers grown on (0001) sapphire substrates used in this work

Chapter 3 Formation of AlN on sapphire surfaces by high-temperature heating in a mixed flow of H_2 and N_2

3.1. Experimental procedure

As Fig. 3-1 shows, a home-built radio-frequency induction furnace which consisted of an atmospheric-pressure horizontal quartz glass tube, a radio-frequency coil (30 kW; 25 kHz), and a tungsten (W) susceptor was used. A mixed gas of H_2 and N_2 with a dew point of –110 °C went through the quartz glass tube at a total flow rate of 10,000 sccm. Here, the molar fraction of H_2 in the mixed gas ($H_2/(H_2 + N_2)$) is denoted by $F°$.

Before placed on the W susceptor, the (0001) sapphire substrate (diameter: 1 inch; thickness: 0.36 mm) was etched in a mixture of 85wt% H_3PO_4 and 97wt% H_2SO_4 (1:3 by volume) at 160 °C for 10 min. It was then rinsed in deionized water and blow-dried by N_2 gas. The sapphire substrate was heated to a temperature which ranged from 980 to 1480 °C. This was done in flowing N_2 ($F° = 0$) to prevent sapphire from decomposing. Heat treatment then started by changing the gas flow to the mixed gas with various values of $F°$. In order not to miss any changes to the substrate surface, a heat-treatment time of 60 min was used in general. After that time, the gas flow was changed to N_2 again, and the substrate was cooled to room temperature (Fig. 3-2). Throughout the experiment, the W susceptor rotated at a rate of 10 rotations per minute. The substrate temperature was measured by a pyrometer that had been calibrated with the melting point of a Si crystal (1414 °C) placed on a sapphire substrate.

Following heat treatment, the surfaces of the sapphire substrates were analyzed by X-ray diffraction (XRD; Spectris, X'Pert MRD) and scanning electron microscopy (SEM;

JEOL, JSM-6700F). To examine the degree of sapphire decomposition and AlN formation, the weights of the substrates were precisely measured before and after heat treatment and after wet chemical etching of surface AlN by potassium hydroxide (KOH) solution after heat treatment.

3.2. Results and discussion

3.2.1. Influence of F° on AlN formation

Fig. 3-3 shows 2θ–ω XRD profiles of the sapphire substrates heat treated at 1330 °C for 60 min for various values of *F*°. Only the diffraction peak from the sapphire (Al_2O_3) substrate is observed at 2θ = 41.675° when *F*° is 0 (N_2 flow) or 1.000 (H_2 flow). On the other hand, diffraction peaks from AlN can be observed clearly at 2θ = 33.225, 36.025, and 37.925° when *F*° is between 0 and 1. These results suggest that undesired AlN appears on the sapphire surface only when H_2 and N_2 coexist in the gas flowing during the high-temperature heat treatment. In addition, the AlN peaks are strong for *F*° between 0.500 and 1.000, implying that the AlN formation is significant within this range.

Fig. 3-4 shows SEM micrographs of the heat-treated sapphire substrates whose XRD profiles are shown in Fig. 3-3. Except for when *F*° = 0 and 1, whiskers of AlN form on the sapphire substrate (Fig. 3-4(b–f)). This is in line with the XRD results in Fig. 3-3. Although AlN formation is not observed when *F*° = 0 and 1 (Fig. 3-4(a) and (g)), the surface becomes rough when *F*° = 1 (Fig. 3-4(g)). This is because the sapphire surface decomposed when H_2 exists (see the discussion in the following paragraph).

To clarify the surface reaction mechanism, the weight of the sapphire substrate was measured with a microbalance (sensitivity: 10 μg) before heat treatment, immediately after heat treatment, and after removing AlN after heat treatment by chemical etching for

2 min using a KOH solution (10 mol/L) which was kept at 60 °C [47]. The amount of AlN that appears on the sapphire substrate during heat treatment can be determined from the difference between the substrate weights immediately after heat treatment and after removal of AlN. On the other hand, the amount of decomposed sapphire during heat treatment can be determined from the difference between the substrate weights before heat treatment and after removal of AlN. Fig. 3-5 shows the influence of $F°$ at a heat-treatment temperature of 1330 °C on the amount of AlN formed and the decomposed sapphire thickness. The AlN was grown on the sapphire substrate like a thicket, so the weight of AlN formed per unit area per hour was plotted in Fig. 3-5. On the other hand, the decomposed sapphire thickness per hour is plotted in Fig. 3-5 because sapphire decomposed uniformly. No decomposition of sapphire was observed when $F° = 0$ (N_2 flow); the thickness of the decomposed sapphire increases as $F°$ increases. Our group has reported that sapphire substrates decompose during heat treatment in flowing H_2 ($F° = 1$) mainly by the following two reactions [48]:

$$Al_2O_3(s) + 3H_2(g) = 2Al(g) + 3H_2O(g), \tag{3-1}$$

$$Al(g) + \frac{1}{2}H_2(g) = AlH(g). \tag{3-2}$$

Because an increase in the H_2 pressure moves the equilibrium of reactions (3-1) and (3-2) to the right, the increase in sapphire decomposition with increasing $F°$ can be understood in a similar way. On the other hand, AlN does not appear when $F° = 0$ or 1, but it does form when H_2 and N_2 coexist ($0 < F° < 1$). The amount of AlN formation is a maximum when $F° \approx 0.75$ (H_2:N_2 = 3:1), as Fig. 3-3 suggests. This suggests the following overall reaction for the heat treatment of sapphire in a mixed flow of H_2 and N_2:

$$Al_2O_3(s) + 3H_2(g) + N_2(g) = 2AlN(s) + 3H_2O(g). \tag{3-3}$$

Subtracting reaction (3-1) from overall reaction (3-3) then leads to the following reaction for the formation of AlN:

$$\mathrm{Al(g)} + \frac{1}{2}\mathrm{N_2(g)} = \mathrm{AlN(s)}. \qquad (3\text{-}4)$$

There, AlN does not form when $F° = 0$. This is because the decomposition of sapphire by reaction (3-1), which is necessary for generating gaseous Al required for the formation of AlN by reaction (3-4), does not take place because H_2 does not exist. On the other hand, AlN does not form when $F° = 1$ because reaction (3-4) does not form AIN due to the absence of N_2, even though gaseous Al is generated by the decomposition of sapphire by reaction (3-1). The above-mentioned results conclude that it is not suitable to use a mixed gas of H_2 and N_2 when a bare sapphire substrate is heated to about 1330 °C.

3.2.2. Influence of heat-treatment temperature on AlN formation

Next, the influence of the heat-treatment temperature of sapphire substrates on the AlN formation was investigated. Fig. 3-6 shows 2θ–ω XRD profiles of sapphire substrates heat treated at various temperatures for 60 min for $F° = 0.750$. In the temperature ranging from 1030 to 1430 °C, we observe diffraction peaks from AlN in addition to the diffraction peak from the sapphire substrate. On the other hand, AlN diffraction peaks are not observed when heat treatment is carried out below 1030 °C or above 1430 °C. These results suggest that AlN appears on a sapphire surface in a certain temperature range.

Fig. 3-7 shows a SEM micrograph of each sample surface whose XRD profile is shown in Fig. 3-6. When the heat treatment is between 1030 and 1430 °C, whiskers of AlN form on the sapphire surface (Fig. 3-7(b–f)). The amount of AlN formation reaches a maximum at about 1330 °C but it is not formed at all when heat treatment is conducted

at 980 °C (Fig. 3-7(a)) or 1480 °C (Fig. 3-7(g)). As described in the following paragraph, the surfaces do not show any changes after the heat treatment at 980 and 1480 °C. The latter surface is decomposed due to the reaction with H_2, whereas the former surface is not decomposed.

Fig. 3-8 shows the influence of the heat-treatment temperature for $F° = 0.750$ on the amount of AlN formation and the thickness of decomposed sapphire. Fig. 3-8 is plotted with the same procedure as was used for Fig. 3-5, in which the substrate weight was measured by a microbalance before and after the heat treatment, and after removing AlN. Sapphire decomposes noticeably above 1130 °C and the thickness of decomposed sapphire increases with increasing heat-treatment temperature. On the other hand, AlN also appeared above 1130 °C. The amount of AlN formation increased as the temperature of the heat treatment went up to 1380 °C; AIN formation then decreased as the heat-treatment temperature further increased. AlN formation was not observed at all at 1480 °C. These trends are in line with the increase in the equilibrium constant (K) of the sapphire decomposition reaction (3-1) with increasing reaction temperature and the decrease in K of the AlN formation reaction (3-4) with increasing reaction temperature (see Table 3-1). Thus, the formation of AlN does not occur below 1030 °C because K of sapphire decomposition reaction (3-1) is extremely small and insufficient gaseous Al, which is required for AlN formation reaction (3-4), is generated, even though K of reaction (3-4) is large enough. On the other hand, AlN does not appear at temperatures above 1430 °C because K of AlN formation reaction (3-4) becomes small even though the increased K of sapphire decomposition reaction (3-1) produces plenty of gaseous Al.

Therefore, the temperature range for the undesirable formation of AlN on a sapphire surface is higher than the general growth temperature range of GaN in MOVPE and HVPE. However, it overlaps the suitable growth temperature range for AlN. Thus, when

AlN directly grows on a sapphire substrate by MOVPE or HVPE at temperatures above 1030 °C, special measures are necessary in order to prevent the undesirable formation of AlN whiskers before heteroepitaxy. For example, to use N_2 alone or a mixture of H_2 and argon (Ar) might be effective, which is thought to control rapid mixing of Al precursors and NH_3 as well as a mixture of H_2 and N_2. The decompression of the VPE reactor might also be effective because the equilibrium of reaction (3-4) shifts to the left.

3.2.3. Thermodynamic analysis

Thermodynamic analysis of the heat treatment of a sapphire substrate in a mixed flow of H_2 and N_2 was carried out to investigate how AlN would form and how sapphire would decompose. Because results were almost identical in the heat treatment of sapphire substrates using a furnace with a resistance heating susceptor made of a graphite element coated with pyrolytic boron nitride, the generation of hydrogen or nitrogen radicals caused by the catalytic effect of the W susceptor was disregarded and the reactions that took place were assumed to be (3-1), (3-2), and (3-4). The following five gaseous species then coexist above the sapphire substrate: H_2, N_2, Al, AlH, and H_2O. The equilibrium equations for reactions (3-1), (3-2), and (3-4) are as follows:

$$K_1 = \frac{P_{\mathrm{Al}}^2 P_{\mathrm{H_2O}}^3}{a_{\mathrm{Al_2O_3}} P_{\mathrm{H_2}}^3}, \tag{3-5}$$

$$K_2 = \frac{P_{\mathrm{AlH}}}{P_{\mathrm{Al}} P_{\mathrm{H_2}}^{1/2}}, \tag{3-6}$$

$$K_3 = \frac{a_{\mathrm{AlN}}}{P_{\mathrm{Al}} P_{\mathrm{N_2}}^{1/2}}, \tag{3-7}$$

where the K_i's show the temperature-dependent equilibrium constants; they can be calculated from NIST-JANAF Thermochemical Tables [49], which are listed in Table 3-

1. The P_i's represent the equilibrium partial pressures of the gaseous species. $a_{Al_2O_3}$ and a_{AlN} are respectively the activities of Al_2O_3 and AlN; they are assumed to be 1 in the current study. The total pressure of the furnace (ΣP_i) is stable, which gives the following equation:

$$\sum P_i = P^o_{H_2} + P^o_{N_2} = P_{H_2} + P_{N_2} + P_{Al} + P_{AlH} + P_{H_2O}, \quad (3\text{-}8)$$

where $P^o_{H_2}$ and $P^o_{N_2}$ are the input partial pressures of H_2 and N_2 to the furnace, respectively. Additionally, hydrogen atoms are not deposited onto a solid, which can lead to the following equation:

$$P^o_{H_2} = P_{H_2} + \frac{1}{2}P_{AlH} + P_{H_2O}. \quad (3\text{-}9)$$

It is possible to obtain the equilibrium partial pressures of gaseous species by solving a set of simultaneous equations (Eqs. (3-5)-(3-9)). In the analysis, the heat-treatment conditions are specified by ΣP_i, $F°$ ($= P^o_{H_2}/(P^o_{H_2} + P^o_{N_2})$), and the temperature.

Because sapphire decomposition reaction (3-1) generates H_2O, the driving force for sapphire formation, $\Delta P_{sapphire}$, can be estimated from the equilibrium partial pressure of H_2O as follows:

$$\Delta P_{sapphire} = -\frac{1}{3}P_{H_2O}. \quad (3\text{-}10)$$

Here, a negative $\Delta P_{sapphire}$ indicates decomposition of sapphire. On the other hand, the driving force for AlN formation, ΔP_{AlN}, can be estimated from the difference between the number of Al atoms sapphire decomposition produces and the amount of Al atoms which remain in the vapor phase as follows:

$$\Delta P_{AlN} = \frac{2}{3}P_{H_2O} - (P_{Al} + P_{AlH}). \quad (3\text{-}11)$$

Fig. 3-9 shows the equilibrium partial pressures of gaseous species over sapphire as a function of $F°$ for atmospheric-pressure heat treatment at 1330 °C. The resultant driving forces for the formation of sapphire and AlN as a function of $F°$ are shown in the lower part of the figure. The equilibrium partial pressure of H_2O, which is a measure of the amount of decomposed sapphire by reaction (3-1), is relatively large above 10^{-5} atm when $F°$ ranges from 0.278 to 0.983 and it rapidly decreases when $F°$ approaches 0 or 1. As the lower part of Fig. 3-9 shows, $\Delta P_{sapphire}$ is 0 when $F° = 0$ and it becomes increasingly negative as $F°$ increases. Its minimum is at $F° = 0.75$ and then increases. $\Delta P_{sapphire}$ is not 0, but -0.0351×10^{-5} when $F° = 1$. These results show that the amount of sapphire decomposition in a mixed gas of H_2 and N_2 is larger than that in flowing H_2 ($F° = 1$) in general, and it becomes a maximum at $F° = 0.75$. This result is not in line with the experimental result shown in Fig. 3-5 where the amount of the sapphire decomposition becomes a maximum when $F° = 1$. The reason for this discrepancy could be because the AlN whiskers form on the sapphire surface when $F°$ is between 0 and 1 and they prevent the reaction between sapphire and H_2.

The equilibrium partial pressures of Al and AlH are lower than the equilibrium partial pressure of H_2O. As $F°$ approaches 0 or 1, the difference between the equilibrium partial pressure of H_2O and the sum of the equilibrium partial pressures of Al and AlH almost disappears. As shown in the lower part of Fig. 3-9, ΔP_{AlN}, which relates to the amount of AlN formation, becomes 0 when $F° = 0$ or 1, while it is positive when $F°$ is between 0 and 1; its maximum value is obtained at $F° = 0.75$. Thus, the dependence of the driving force for AlN formation on $F°$ obtained by the thermodynamic analysis is in line with the experimental result Fig. 3-5 shows, where the amount of AlN formation also becomes a maximum at $F° \approx 0.75$.

Fig. 3-10 shows the heat-treatment temperature dependence of the equilibrium partial pressures of the gaseous species over sapphire and the resulting driving forces for sapphire and AlN formation. The upper part of Fig. 3-10 shows that the equilibrium partial pressure of H_2O gradually increases as heat-treatment temperature increases. The lower part of the figure indicates that $\Delta P_{sapphire}$ becomes increasingly negative as heat-treatment temperature goes up. This implies that more sapphire decomposes with increasing heat-treatment temperature. This corresponds to the experimental result shown in Fig. 3-8. On the other hand, the equilibrium partial pressures of Al and AlH increase rapidly as heat-treatment temperature increases, and they become almost equal to the equilibrium partial pressure of H_2O at about 1800 °C because K of reaction (3-4) decreases with increasing heat-treatment temperature. In the lower part of Fig. 3-10, ΔP_{AlN} increases as heat-treatment temperature goes up and it becomes a maximum at 1608 °C, and then decreases with further increase in the heat-treatment temperature. Finally, ΔP_{AlN} becomes negative at a heat-treatment of 1724 °C or above; as a result, AlN does not appear in this temperature range. Though the tendency of the temperature dependence of ΔP_{AlN} corresponds to that of AlN formation shown in Fig. 3-8, the temperature at which ΔP_{AlN} becomes a maximum (1608 °C) is higher than the experimental result (1380 °C). This discrepancy may be due to the fact that AlN does not readily adhere to the decomposing sapphire surface at high temperatures. Therefore, the decomposition of sapphire substrates and the formation of AlN on sapphire surfaces while heat treatment is conducted in a mixed flow of H_2 and N_2 can be explained in terms of thermodynamics.

3.3. Conclusions

Heat treatment of (0001) sapphire substrates in atmospheric-pressure mixed flows of H_2 and N_2 with various molar fractions of H_2 ($F° = H_2/(H_2 + N_2)$) was investigated where the temperature ranged from 980 to 1480 °C. When H_2 and N_2 coexisted in the flowing gas ($0 < F° < 1$) at 1330 °C, undesirable AlN whiskers appeared on sapphire surfaces. This is because H_2 generates gaseous Al in reaction to the sapphire, and this gaseous Al reacts with N_2 to form AlN. It was found that the amount of the AlN formation was a maximum at $F° = 0.750$. On the other hand, for $F° = 0.750$, AlN whiskers formed in the temperature which ranged from 1030 to 1430 °C and the formation of AlN was the largest at 1380 °C. The experimental results were explained by thermodynamic analysis of the system. Thus, the mixed gas of H_2 and N_2 is not considered an appropriate flowing gas when a bare sapphire is used for heteroepitaxy of AlN at high temperatures above 1030 °C.

Figures and a table

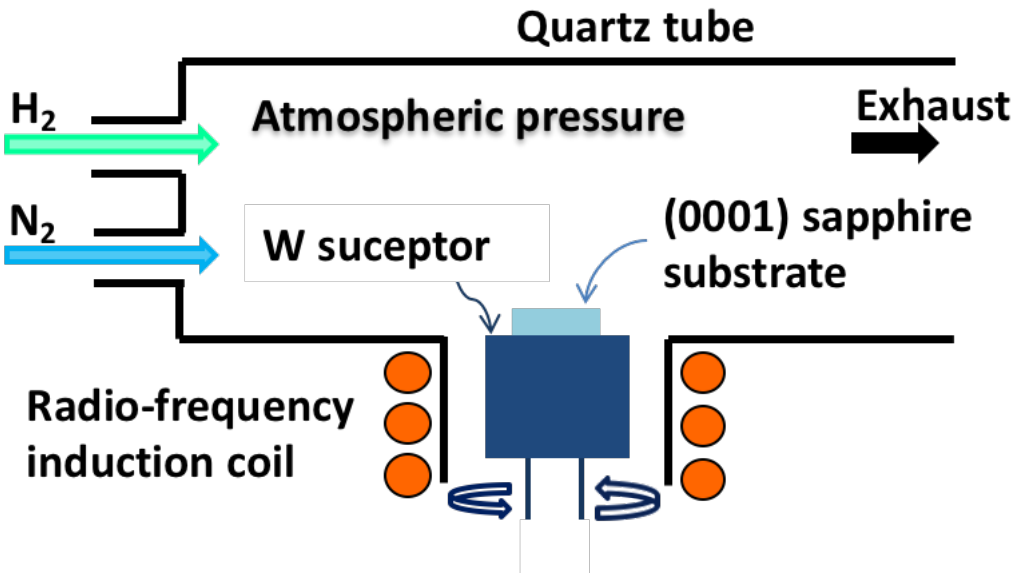

Fig. 3-1. Schematic diagram of the home-built radio-frequency induction furnace used in Chapters 3 and 4.

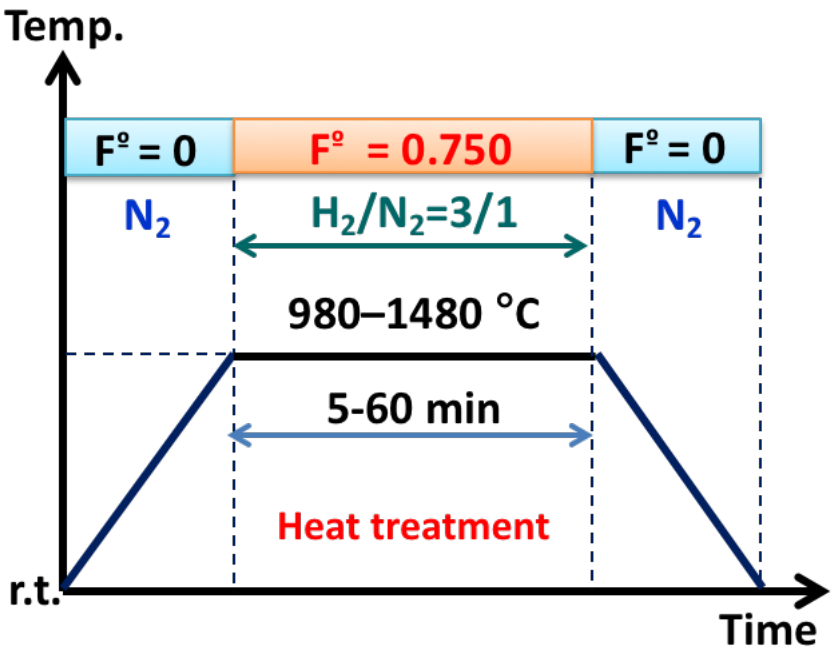

Fig. 3-2. Temperature profile and flowing gas for experiments in Chapters 3 and 4.

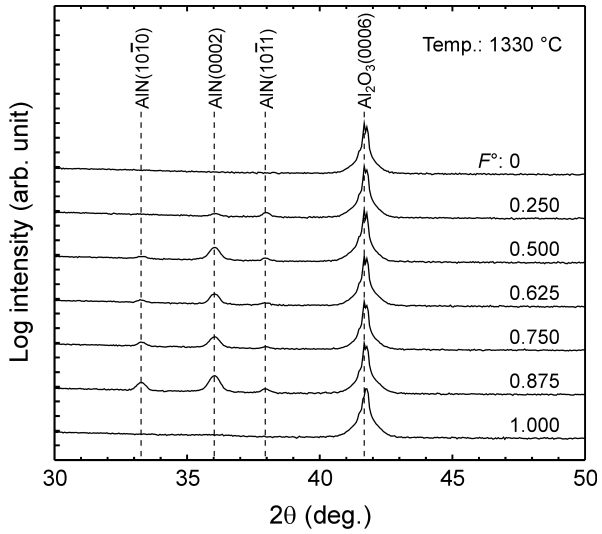

Fig. 3-3. 2θ–ω XRD profiles of sapphire substrates after 60 min heat treatment at 1330 °C in gas flows with various values of *F*°.

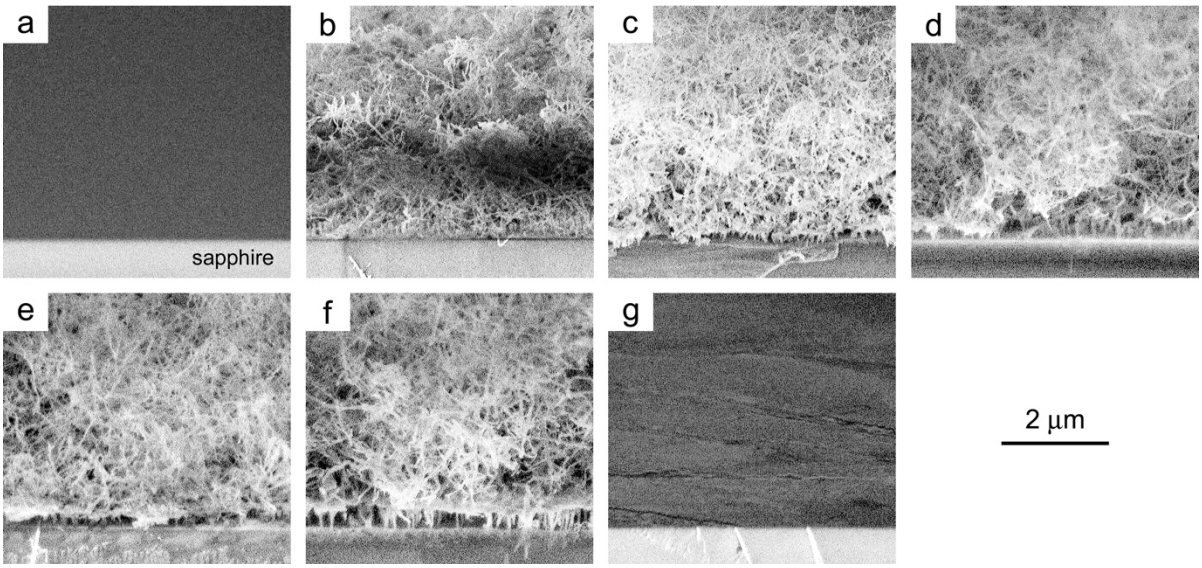

Fig. 3-4. SEM micrographs of (0001) sapphire substrates after 60 min heat treatment at 1330 °C in gas flows with various values of $F°$: (a) 0, (b) 0.250, (c) 0.500, (d) 0.625, (e) 0.750, (f) 0.875, and (g) 1.000.

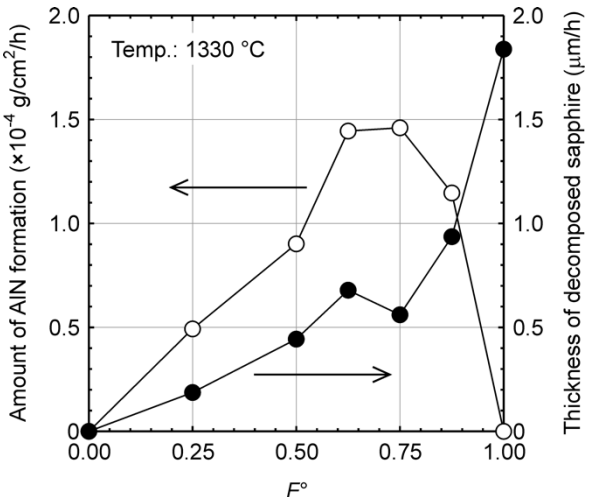

Fig. 3-5. Influence of *F*° on AlN formation and sapphire decomposition during heat treatment of sapphire substrate at 1330 °C.

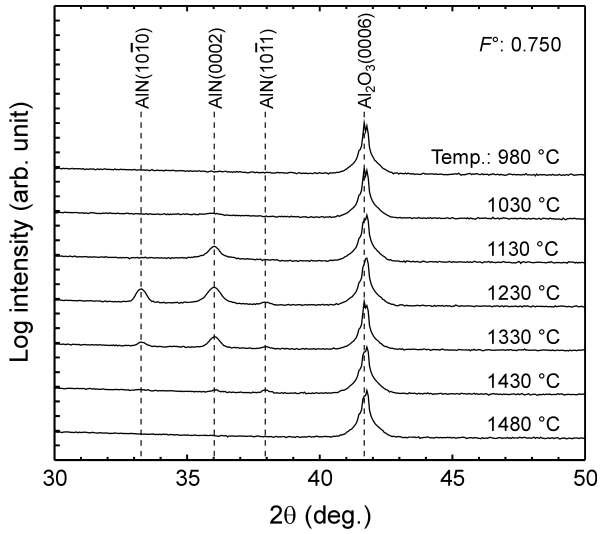

Fig. 3-6. 2θ–ω XRD profiles of sapphire substrates heat treated at various temperatures for 60 min in gas flow with F° = 0.750.

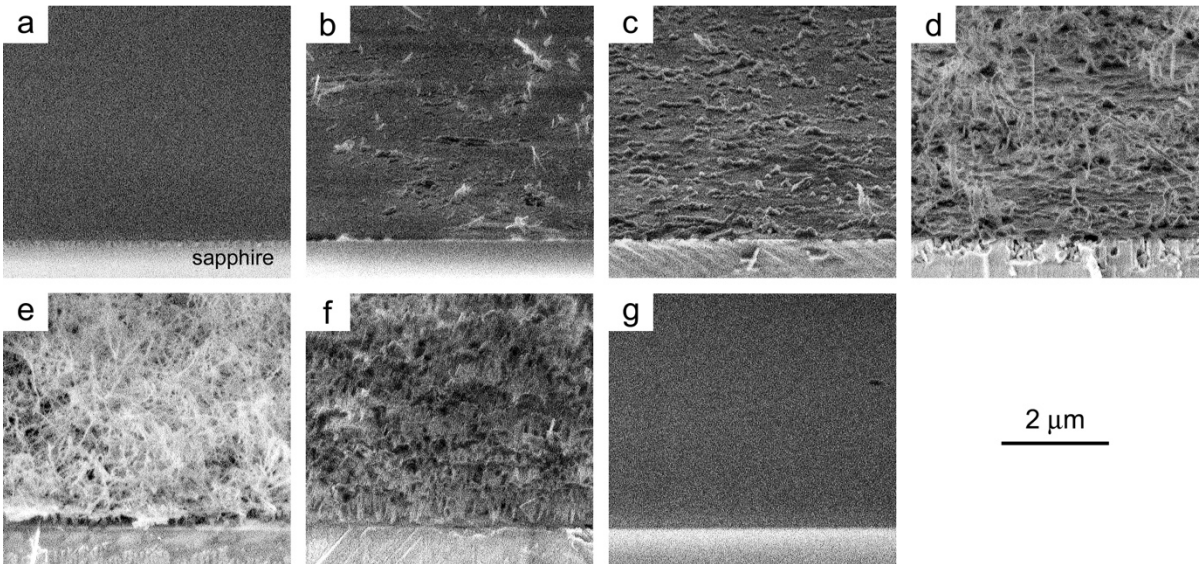

Fig. 3-7. SEM micrographs of (0001) sapphire substrates after 60 min heat treatment for $F°$ = 0.750 at temperatures of (a) 980, (b) 1030, (c) 1130, (d) 1230, (e) 1330, (f) 1430, and (g) 1480 °C.

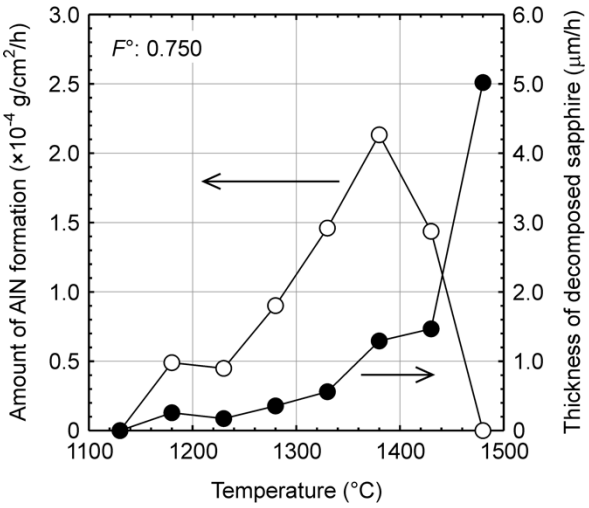

Fig. 3-8. Influence of heat-treatment temperature on AlN formation and sapphire decomposition during heat treatment of sapphire substrate for $F° = 0.750$.

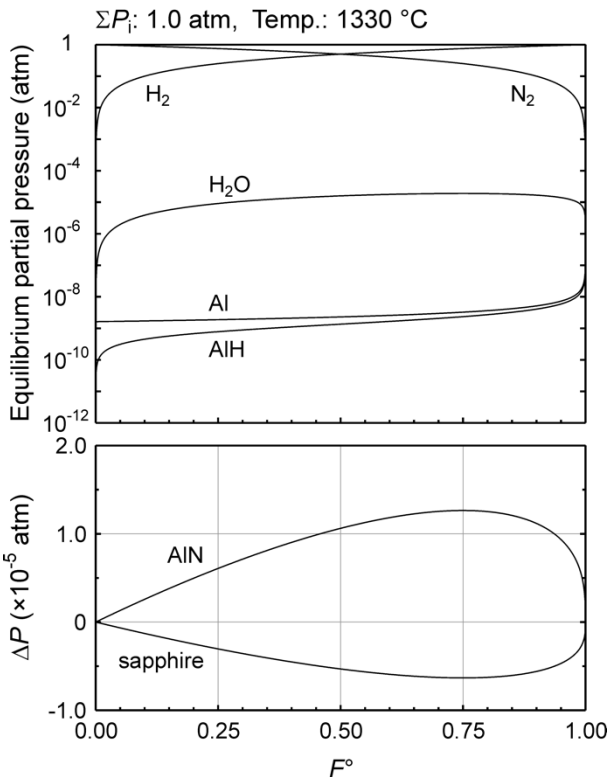

Fig. 3-9. Equilibrium partial pressures of gaseous species over a sapphire substrate as a function of $F°$ (upper) and resultant driving forces of sapphire and AlN formation (lower) calculated for atmospheric-pressure heat treatment at 1330 °C.

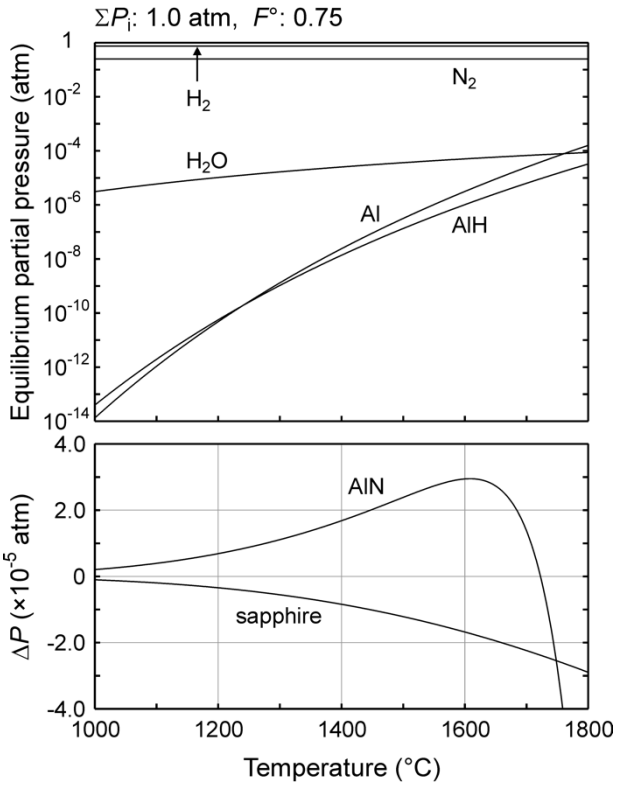

Fig. 3-10. Heat-treatment temperature dependence of equilibrium partial pressures of gaseous species over a sapphire substrate (upper) and resultant driving forces of sapphire and AlN formation (lower) calculated for atmospheric-pressure heat treatment for F° = 0.75.

Reactions	$\mathrm{Log}_{10}K$
$Al_2O_3(s) + 3H_2(g) = 2Al(g) + 3H_2O(g)$	$40.7 - 8.49\times10^4 / T - 5.78\times\log_{10} T$
$Al(g) + \frac{1}{2}H_2(g) = AlH(g)$	$-1.59 + 3.67\times10^3 / T - 2.43\times10^{-1}\times\log_{10} T$
$Al(g) + \frac{1}{2}N_2(g) = AlN(s)$	$-16.1 + 3.41\times10^4 / T + 1.13\times\log_{10} T$

Table 3-1. Equations of equilibrium constants *K's* of the reactions as a function of temperature *T* (K).

Chapter 4 Formation mechanism of AlN whiskers on sapphire surfaces heat-treated in a mixed flow of H_2 and N_2

4.1. Experimental procedure

The heat treatment of sapphire substrates was conducted in order to investigate the whisker formation mechanism by using an atmospheric-pressure horizontal quartz-glass furnace which was equipped with a radio-frequency (30 kW; 25 kHz) induction heating system (Fig. 3-1). Before the heat treatment, (0001) sapphire substrates were etched in a mixed acidic solution of 85 wt% H_3PO_4 and 97 wt% H_2SO_4, 1 to 3 by volume, at 160 °C for 10 min. After being rinsed in deionized water and dried, each sapphire substrate was put on the induction heating susceptor made of tungsten, which was rotated at a rate of 10 rotations per minute for higher uniformity.

Then, the (0001) sapphire substrate was heated to the desired temperature, which ranged from 980–1380 °C in N_2 ($F°$ = 0) to prevent sapphire from decomposing, and it was maintained at the maximum temperature for 5 to 60 min in the mixed flow of H_2 and N_2 with $F°$ of 0.750. After the retention time, the substrate was cooled to room temperature in N_2 ($F°$ = 0). The total gas flow rate was 10000 sccm throughout the process. An optical pyrometer monitored the substrate temperature (Fig. 3-2).

After the heat treatment, the sapphire substrates were analyzed by scanning electron microscopy (SEM; JEOL JSM-6700F) and X-ray diffraction (XRD; Spectris X'Pert MRD). The quantitative analysis of sapphire decomposition and AlN formation was carried out by weighing samples before and after heat treatment, and after the removal of AlN by using KOH aqueous solution [47].

4.2. Results and discussion

AlN whisker formation was observed above 1030 °C in the mixed flow of H_2 and N_2 with $F°$ of 0.750, and the amount of AlN whiskers increased as heat-treatment temperature went up. The SEM observation (Fig. 4-1) and XRD measurements (Fig. 4-2) of sapphire substrates heat-treated at 1380 °C for 5 to 20 min were performed. As shown in Fig. 4-1, AlN whiskers formed on sapphire substrates which was heated for 20 min, whereas the $2\theta/\omega$ scan XRD profiles in Fig. 4-2 revealed that AlN existed on sapphire substrates heated for 5 min or longer. These results indicate that the thin c-axis-oriented AlN layer formed first after being heated for 5 min, although the AlN layer could not be seen clearly by SEM. The morphology change of the sapphire surface was also observed for the sample heated for 10 min, implying the formation of the thin AlN layer on the sapphire surface. Cross-sectional SEM observation revealed that the AlN layer was 89 nm thick. These results confirmed that the AlN film first covered sapphire substrates, and then AlN whiskers began to form.

Both amounts of sapphire decomposition and AlN formation, calculated by weighing samples before and after the heat treatment, and after the removal of AlN by using KOH aqueous solution (10 mol/L), increased with heat-treatment time (Fig. 4-3). This suggests that AlN formation resulted from sapphire decomposition.

The next experiment was performed by lowering the heat-treatment temperature to 1130 °C so that the reaction rate would decrease. Fig. 4-4 shows SEM surface micrographs of the sapphire substrate taken after heat treatment at 1130 °C for 60 min (Fig. 4-4(a)) and taken after the subsequent removal of AlN by using KOH aqueous solution (Fig. 4-4(b)). It was found that pits formed on the sapphire surface beneath the

thin AlN layer after heat treatment. It is notable that the pits on sapphire surface beneath the thin AlN layer are seen indistinctly on the as-heat-treated surface in Fig. 4-4(a). Both the number of AlN whiskers on the as-heat-treated surface and the number of pits on the sapphire surface were counted manually with SEM micrographs (Fig. 4-4). Densities of whiskers and pits were 8.9×10^8 and 7.5×10^8 cm^{-2}, respectively. Because both numbers were on the same order of magnitude, this strongly suggested that the formation of AlN whiskers resulted from the pit formation. In other words, AlN whiskers formed as sapphire decomposed.

From the results above, the formation mechanism of AlN whiskers on sapphire surfaces when heated in a mixed flow of H_2 and N_2 could be explained schematically in Fig. 4-5. First, gaseous Al is generated by H_2 in flowing gas through a reaction with sapphire by the following reaction (Fig. 4-5(a)):

$$Al_2O_3(s) + 3H_2(g) = 2Al(g) + 3H_2O(g). \quad (4\text{-}1)$$

The gaseous Al immediately reacts with N_2 in flowing gas and a thin AlN layer is formed on the sapphire surface by the following reaction (Fig. 4-5(b)):

$$2Al(g) + N_2(g) = 2AlN(s). \quad (4\text{-}2)$$

Then, H_2 preferentially diffuses to the AlN/sapphire interface via dislocations in the thin AlN layer and reacts with sapphire. The reaction between sapphire and H_2 produces gaseous Al, also diffuses through dislocations in the thin AlN layer and leaves pits on the sapphire surface (Fig. 4-5(c)). Finally, as Fig. 4-5(d) shows, the gaseous Al immediately reacts with N_2 in flowing gas to form AlN whiskers on the thin AlN layer (reaction (4-2)). Thus, both AlN whisker and pit densities on the sapphire surface are almost the same, as shown in Fig. 4-4. These densities (on the same order of 10^8 cm^{-2}) are reasonable considering the dislocation density of the AlN layer directly grown on sapphire by metalorganic chemical vapor deposition (MOCVD). What is interesting is the formation

mechanism of pits on the sapphire surface is similar to that of voids beneath the thin AlN buffer layer during post-growth heat treatment in a mixed flow of H_2 and N_2 [31]. The bird's-eye view SEM image (Fig. 4-5(e)) provides another piece of evidence that supports the hypothesis described above; that is, both sapphire decomposition beneath the thin AlN layer and AlN formation, which occur simultaneously, results in the continuous growth of AlN whiskers.

4.3. Conclusions

We investigated the formation mechanism of AlN whiskers on (0001) sapphire substrates in the temperature ranging from 980–1380 °C in an atmospheric-pressure mixed flow of H_2 and N_2 with $F°$ of 0.750 (H_2/N_2 = 3/1). The results suggested that the sapphire surface reacts with H_2, and the Al gas generated forms an AlN thin layer on the surface by reacting with N_2. Then, H_2 diffuses to the AlN/sapphire interface and reacts with sapphire, the generated Al gas escapes via dislocations in the thin AlN film to leave pits on the sapphire surface; moreover, the Al gas immediately reacts with N_2 to form AlN whiskers on the thin AlN layer. Thus, it has been confirmed that a mixed flow of H_2 and N_2 is unsuitable for the heteroepitaxial growth of AlN on sapphire substrates in view of preventing the undesirable formation of impeditive AlN whiskers before AlN growth. It is expected that this finding will significantly contribute to the realization of large-diameter bulk AlN.

Figures

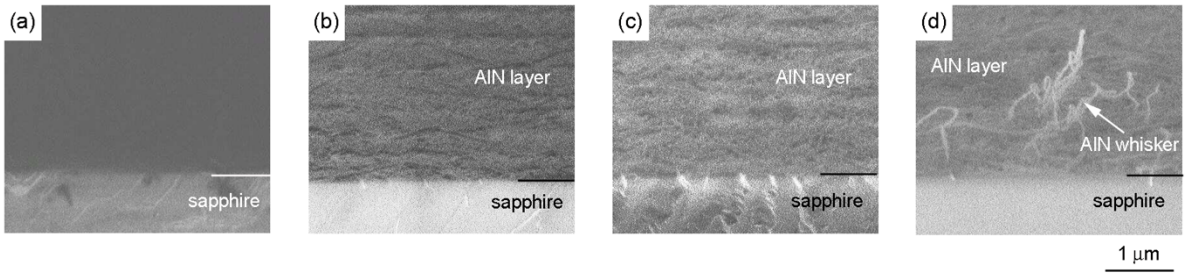

Fig. 4-1. Bird's-eye view SEM micrographs of (0001) sapphire substrates before heat treatment (a) and after heat treatment in a mixed gas flow with $F°$ = 0.750 (H_2/N_2 = 3/1) at 1380 °C for (b) 5, (c) 10, and (d) 20 min.

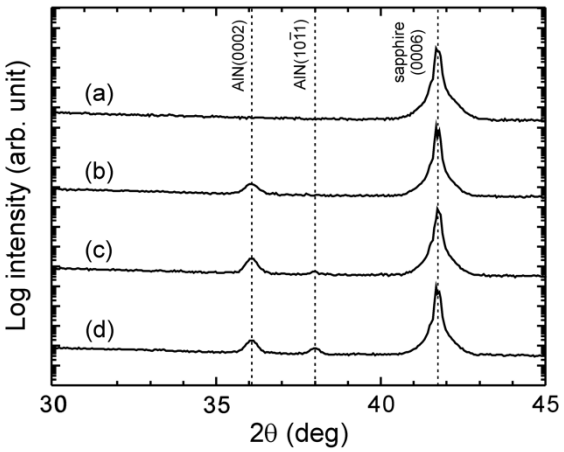

Fig. 4-2. 2θ/ω scan XRD profiles of sapphire substrates before heat treatment (a) and after heat treatment in a mixed gas flow with $F°$ = 0.750 (H_2/N_2 = 3/1) at 1380 °C for (b) 5, (c) 10, and (d) 20 min.

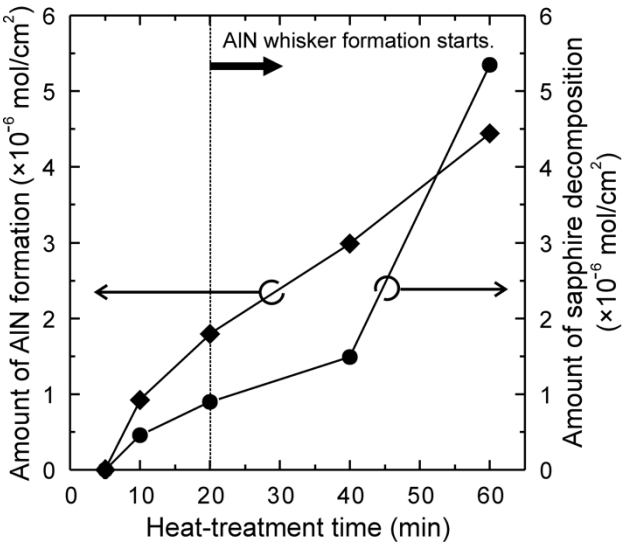

Fig. 4-3. Amounts of AlN layer and whisker formation and sapphire decomposition versus heat-treatment time at 1380 °C in a mixed gas flow with $F° = 0.750$.

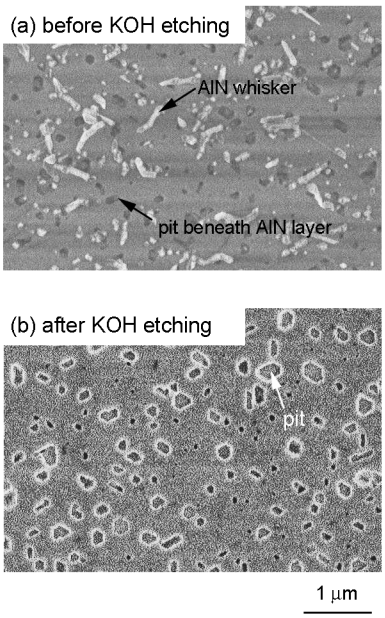

Fig. 4-4. SEM micrographs of sapphire substrate heat-treated at 1130 °C for 60 min in a mixed gas flow with $F^{\circ} = 0.750$: (a) as-heat-treated surface before KOH etching and (b) sapphire surface after the removal of AlN by KOH etching.

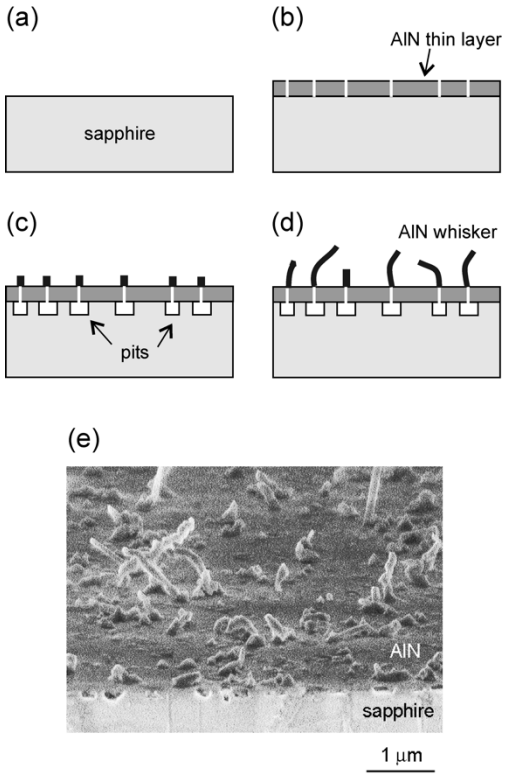

Fig. 4-5. Schematic section drawings explaining formation of AlN whiskers (a)-(d), and bird's-eye view SEM micrographs of sapphire substrate heat-treated at 1130 °C for 60 min showing simultaneous formation of AlN whiskers and pits beneath thin AlN layer (e).

Chapter 5 Investigation of void formation beneath thin AlN layers by decomposition of sapphire substrates for self-separation of thick AlN layers grown by HVPE

5.1. Experimental procedure

A homebuilt HVPE system [37], which was comprised of an atmospheric pressure horizontal hot-wall quartz glass reactor, a multi-zone electric furnace, and a resistive heating susceptor which is capable of heating the substrate directly up to 1500 ºC was used (Fig. 5-1). AlN growth was carried out with $AlCl_3$ and NH_3 as source gases. A mixture of H_2 and N_2 (H_2/N_2 = 7/3) with a dew point below –110 ºC was commonly used as carrier gas. The introduction of HCI gas over the Al metal (6N-grade), which was kept at 500 ºC, generated $AlCl_3$ in the upstream region of the reactor (source zone) [36]. $AlCl_3$ and NH_3 were separately introduced into the downstream region (growth zone) maintained at 540 ºC, where the resistive heating susceptor was placed to grow AlN at a selected temperature.

The (0001) sapphire substrate (5.2 × 3.4 × 0.40 mm^3) was etched in a solution of H_3PO_4/H_2SO_4 (= 1/3, v/v) at 160 ºC for 10 min and later rinsed in deionized water before it was set on the resistive heating susceptor. Firstly, an intermediate 50 to 200 nm thick AlN layer was grown at 1065 ºC, at which temperature the decomposition reaction of sapphire with H_2 is insignificant [39], with $AlCl_3$ and NH_3 input partial pressures of 5.0 × 10^{-4} and 1.3 × 10^{-3} atm, respectively. $AlCl_3$ was normally preflowed (5.0 × 10^{-4} atm) for 2 min to saturate the substrate surface with Al before the intermediate AlN layer grew. Secondly, the substrate was raised to a temperature between 1300 and 1450 ºC in a H_2/N_2

mixed carrier gas (H_2/N_2 = 7/3) flow with added NH_3 at an input partial pressure of 1.3×10^{-3} atm, and then heat-treated for specific time to form voids under the intermediate AlN layer. For comparison, heat treatment was also carried out in a gas flow of N_2 carrier gas or N_2 carrier gas with added NH_3 at an input partial pressure of 1.3×10^{-3} atm. Finally, thick AlN layers were grown at 1450 ºC for 4 h with $AlCl_3$ and NH_3 input partial pressures of 5.0×10^{-4} and 2.0×10^{-3} atm, respectively. After the growth of AlN layers, the substrate was cooled to RT with a supply of NH_3 to prevent AlN from decomposing.

5.2. Results and discussion

5.2.1. Void formation beneath the intermediate AlN layer

Heat treatment of sapphire substrates which were covered with thin intermediate AlN layers was investigated in various gas flows. Fig. 5-2 shows cross-sectional scanning electron microscopy (SEM) micrographs of 100 nm thick AlN/sapphire interfaces obtained after heated at 1450 ºC for 30 min in a gas flow of N_2 carrier gas, H_2/N_2 mixed carrier gas with added NH_3 or N_2 carrier gas with added NH_3. The interface did not change after the heat treatment in the N_2 carrier gas (Fig. 5-2(a)). On the other hand, when the heat treatment was carried out in the H_2/N_2 mixed carrier gas with added NH_3, many voids developed under the AlN layer by decomposition of the sapphire substrate (Fig. 5-2(b)), while no decomposition of AlN took place, because NH_3 existed [50]. These results indicate that hydrogen can diffuse through the thin AlN layer to the AlN/sapphire interface, where it reacts with sapphire. As Fig. 5-2(b) shows, each void is almost equally deep, and extends laterally with a (0001) bottom plane and $\{10\bar{1}2\}$ or $\{10\bar{1}0\}$ sidewalls. This result is consistent with a greater decomposition rate of sapphire by reaction with H_2 on the $\{10\bar{1}2\}$ plane than on the (0001) plane [48]. Furthermore, it was found that voids

formed beneath the AlN layer when the heat treatment was performed in the N_2 carrier gas with added NH_3 (Fig. 5-2(c)), similar to heat treatment in the H_2/N_2 mixed carrier gas with added NH_3. This is considered to be because of the thermal decomposition of a small amount of NH_3 to N_2 and H_2, which leads to the same effect as heat treatment in the H_2/N_2 mixed carrier gas with added NH_3. It is important to note that the ratio of NH_3 decomposition is considered to be very low, because HVPE of AlN is possible even at 1450 ºC [38]. The only difference between heat treatment in the N_2 carrier gas with added NH_3 and in the H_2/N_2 mixed carrier gas with added NH_3 was that three-dimensional AlN islands regrew on the top of the AlN layer when the heat treatment was performed in N_2 carrier gas with added NH_3. Our group reported that the sapphire decomposed by reaction with H_2, mainly by the following chemical reaction above 1300 ºC [48]:

$$Al_2O_3(s) + 3H_2(g) = 2Al(g) + 3H_2O(g). \quad (5\text{-}1)$$

Gaseous Al generated by reaction (5-1) can further react with NH_3 in the atmosphere, which causes AlN to regrow by the following chemical reaction:

$$Al(g) + NH_3(g) = AlN(s) + \frac{3}{2}H_2(g). \quad (5\text{-}2)$$

Fig. 5-2(c) shows the regrowth of AIN. The reason for its regrowth is that few H_2 molecules exist in the atmosphere, which consequently shifts the equilibrium of the chemical reaction (5-2) to the right. On the contrary, AlN hardly regrows when the heat treatment is carried out in the H_2/N_2 mixed carrier gas with added NH_3 (Fig. 5-2(b)), because an increased concentration of H_2 in the atmosphere moves the equilibrium of reaction (5-2) to the left. Additionally, the surface of the intermediate AlN layer was (0001) AlN, and the full-widths at half-maximum (FWHMs) from X-ray diffraction (XRD) rocking curves for symmetric (0002) AlN and asymmetric ($10\bar{1}0$) AlN planes were not markedly different after heat treatments in various gas flows (FWHMs were 19

and 58 arcmin for (0002) AlN and ($10\bar{1}0$) AlN planes, respectively). This suggests that the H_2/N_2 mixed carrier gas with added NH_3 is suitable as a flowing gas to form voids beneath thin AlN layers. The segment ratio of voids at the interface R_v, is defined by the following expression:

$$R_v = \frac{\sum L_{void}}{L_{interface}}, \tag{5-3}$$

in which $L_{interface}$ is the length of the interface and L_{void} is the length of each void along the [$1\bar{1}00$] direction of sapphire. Although there was a difference in the H_2 concentration in the atmosphere, almost the same R_v values were obtained after heat treatment in the H_2/N_2 mixed carrier gas with added NH_3 (R_v = 49.8%) and in N_2 carrier gas with added NH_3 (R_v = 47.1%). This result shows that hydrogen diffuses to the interface very fast. It also indicates that the formation of voids is limited by the diffusion of gaseous Al or H_2O generated by the decomposition of sapphire to the surface, which suggesting that void formation could be controlled depending on the temperature, the duration of heat treatment, and the thickness of the AlN layer.

Next, the influence of heat treatment temperature on the formation of voids beneath the intermediate AlN layer was investigated. Fig. 5-3 shows cross-sectional SEM micrographs of 100 nm thick AlN/sapphire interfaces after 30 min heat treatment at various temperatures in the H_2/N_2 mixed carrier gas with added NH_3. Each micrograph shows the values of R_v and average depths of voids D_v, after each heat treatment. The interface before the heat treatment and after heat treatment at 1300 ºC was almost the same. However, significant void development took place under the AlN layer with heat treatment at higher temperatures above 1400 ºC. Thus, heat treatment at 1400 ºC or above is crucial to form voids beneath the AlN layer with significant R_v values. The R_v value and the areal ratio of voids at the interface were almost equal, as described later. Therefore,

the value of $R_v \cdot D_v$ at each heat treatment temperature indicates the volume of decomposed sapphire, and an activation energy of 883 kJ/mol was obtained from an Arrhenius plot of $R_v \cdot D_v$. The activation energy (883 kJ/mol) is much larger than the energy needed for the decomposition reaction between (0001) sapphire (362 kJ/mol) or $(10\bar{1}2)$ sapphire (349 kJ/mol) and H_2 [48]. Thus, it is considered that the activation energy is the one for the diffusion of gaseous Al or H_2O generated by sapphire decomposition, as discussed in Fig. 5-2.

The diffusion path of gaseous Al and/or H_2O in the intermediate AlN layer was also investigated. Fig. 5-4 shows surface SEM micrographs of a 100 nm thick AlN/sapphire sample heat-treated in the H_2/N_2 mixed carrier gas with added NH_3 at 1450 ºC for 30 min during the process of etching in potassium hydroxide (KOH) solution. Just after the heat treatment, the surface of the AlN layer was found to be smooth and free of pitting (Fig. 5-4(a)); however, many pits were generated on the AlN surface after 2 min etching in KOH solution (Fig. 5-4(b)). The density of pits on the surface was 1.6×10^9 cm^{-2}. Yazdi *et al.*'s study reported that the density of pits on an AlN surface which was etched in hot KOH solution corresponds well to that of the dislocations estimated by transmission electron microscopy (TEM) analysis [51]. Thus, the pits on the surface of AlN in Fig. 5-4(b) are thought to correspond to the dislocations in the intermediate AlN layer. Furthermore, after the AlN layer was completely removed, many hexagonal-shaped hollows surrounded by $\{10\bar{1}2\}$ or $\{10\bar{1}0\}$ planes of sapphire were observed on the sapphire surface (Fig. 5-4(c)). These hollows correspond to the voids in the cross-sectional observations of the AlN/sapphire interface, and the areal ratio of hollows (voids) at the interface and the segment ratio of voids at the interface, R_v, were almost equal. In addition, the density of hollows (1.8×10^9 cm^{-2}) was almost equal to the pit density at the

AlN surface; thus, the voids are thought to be located under the pits, and the dislocations in AlN are possible paths for the diffusion of gaseous Al and/or H_2O to the AlN surface.

The influence of the source gas supply sequence for the growth of the intermediate AlN layer on the formation of voids was then investigated. Fig. 5-5 shows cross-sectional SEM micrographs of 100 nm thick AlN/sapphire interfaces after 30 min heat treatment at 1450 ºC in the H_2/N_2 mixed carrier gas with added NH_3. The source gas supply sequence was (a) $AlCl_3$ preflow for 2 min (usual procedure), (b) simultaneous supply of $AlCl_3$ and NH_3, and (c) NH_3 preflow for 2 min. Many voids formed beneath the AlN layer if $AlCl_3$ was flowed before the AlN layer grew (Fig. 5-5(a)); however, very few voids formed when $AlCl_3$ and NH_3 were simultaneously supplied (Fig. 5-5(b)), or when NH_3 was flowed before the AlN layer grew (Fig. 5-5(c)). Thus, the formation of voids beneath the AlN layer strongly depends on the source gas supply sequence for the growth of the intermediate AlN layer. The FWHMs of the XRD rocking curves for the symmetric (0002) AlN and asymmetric ($10\bar{1}0$) AlN planes were 19 and 58 arcmin for the samples as shown in Figs. 5-5(a) and 3-5(b), respectively, while those for the sample in Fig. 5-5(c) were 6 and 118 arcmin, respectively. This means that void formation was suppressed when $AlCl_3$ and NH_3 were simultaneously supplied or when NH_3 was flowed before the growth of AlN layer, even though many dislocations were contained in the AlN layer. The lattice polarity of the AlN layers revealed by etching in KOH solution [42] was Al-polarity for Figs. 5-5(a) and 5-5(b), and N-polarity for Fig. 5-5(c). These results indicate that the suppression of void formation is not because of the growth of an N-polarity AlN layer, but because of nitridation of sapphire surface before the growth of the AlN layer. The surface of a sapphire substrate is uniformly nitrided by heating at 1050 ºC in an NH_3-containing gas flow [52]. Furthermore, Fukuyama *et al.* reported that a thin single crystalline AlN layer with no threading dislocations could grow by high temperature

nitridation of the sapphire substrate surface [53]. Therefore, it is considered that a thin nitrided layer of sapphire which has no dislocations forms between the intermediate AlN layer and the sapphire substrate when $AlCl_3$ is not flowed before the AlN layer grows, and this may impede the diffusion path of gaseous Al and/or H_2O, and thereby void formation is suppressed. Thus, preflow of $AlCl_3$ for the growth of the intermediate AlN layer is crucial for subsequent formation of voids beneath the AlN layer.

Finally, with an aim to control the R_v value for subsequent growth and self-separation of thick AlN layers, the influence of the intermediate AlN layer thickness and heat treatment time on the formation of voids beneath the AlN layer was investigated. Fig. 5-6 shows cross-sectional SEM micrographs of AlN/sapphire interfaces with AlN thicknesses between 50 and 200 nm after 15–60 min heat treatment at 1450 ºC in the H_2/N_2 mixed carrier gas with added NH_3. Each micrograph shows the values of R_v and D_v. When the thickness of the AlN layer remained the same, voids extended and mutually coalesced as the heat treatment time increased. When the heat treatment time was fixed, on the other hand, the voids were significantly extended as the AlN layer thickness decreased. Therefore, the ease of diffusion of gaseous Al and/or H_2O in the AlN layer correlates negatively with the thickness of the AlN layer. AlN above a wide void sinks into the void when the AlN layer is thin and R_v is large, as shown in Fig. 5-6(d). For the following growth of thick AlN layers after void formation, the sinking of the intermediate AlN layer into the voids is thought to be a critical problem. Furthermore, when a 50 nm thick AlN/sapphire sample was heat-treated for 60 min (Fig. 5-6(g)), the AlN layer fully separated from the sapphire substrate ($R_v = 100\%$) while the heat treatment was conducted. At the same time, the thickness of the AlN layer increased as AlN regrew. The reason for the regrowth of AlN during heat treatment is that there was a shift of the equilibrium of reaction (5-2) to the right by the increase of gaseous Al, because the full separation of the

AlN layer during heat treatment causes sapphire to decompose directly in the presence of H_2.

The dependence of R_v on the thickness of the intermediate AlN layer and heat treatment time was examined when AlN layer thickness ranged from 50 to 200 nm and when heat treatment times changed from 1 to 60 min to produce the R_v chart, which was shown in Fig. 5-7. The R_v chart indicates that to shorten or to extend the heat treatment duration is necessary in order to achieve a desirable R_v value, when the AlN layer thickness is thin and thick, respectively. Therefore, this chart is particularly useful to control void formation beneath thin AlN layers before subsequent growth of thick AlN layers for the preparation of freestanding AlN substrates.

5.2.2. Self-separation of thick AlN layer from a sapphire substrate

Thick AlN layers was grown at 1450 ºC for 4 h on intermediate AlN layers of various thickness and R_v values in order to investigate how thick AlN layers themselves separate from sapphire substrates via interfacial voids. Fig. 5-8 is a photograph of the self-separated freestanding (0001) AlN substrates (a–c) obtained using intermediate AlN layers with void formations as those shown in Figs. 5-6(a), (e) and (i), respectively. The freestanding AlN substrates were placed on paper, where the characters "AlN" were printed. The freestanding AlN substrates was 79 μm thick, which reflects an average growth rate of 19.7 μm/h. The freestanding AlN substrate of Fig. 5-8(a) grown on a 50 nm thick intermediate AlN layer with R_v of 45.9% self-separated from sapphire substrate during growth at 1450 ºC because the 50 nm thick AlN layer is fragile with voids beneath it. The grown layer cracked to produce some flakes, so that a freestanding AlN substrate with the same size as the sapphire substrate used was not obtained. Moreover, the obtained freestanding AlN substrate became cloudy, suggesting the oxygen

contamination from the H_2O which was generated by the decomposition of the sapphire substrate and/or due to the roughness on the surface of the freestanding AlN substrate. On the other hand, the thick AlN layer grown on an intermediate AlN layer at 100 nm thick and with R_v of 49.8% or at 200 nm thick with R_v of 38.0% self-separated during post-growth cooling of the sapphire substrate to RT with the aid of voids at the interface. Therefore, transparent freestanding AlN substrates of the same size as the sapphire substrate were obtained, as shown in Figs. 5-8(b) and 5-8(c). Although not shown here, the self-separation of a thick AlN layer from a sapphire substrate did not occur when a 100 nm thick intermediate AlN layer with R_v of less than 20% was used, but cracks were generated in both the AlN layer and sapphire substrate [54].

The surface morphology of the freestanding AlN substrates shown in Fig. 5-8 was observed by SEM. Fig. 5-9 shows bird's-eye view SEM micrographs of freestanding AlN substrates showing the (0001) surface and $(10\bar{1}0)$ cleaved plane. The surface of the freestanding AlN substrate that self-separated during growth (Fig. 5-8(a)) was rough, as shown in Fig. 5-9(a), which might be due to a decrease of the effective growth temperature of the thick AlN layer. On the other hand, the freestanding AlN substrates that self-separated from the sapphire substrates during post-growth cooling to RT (Figs. 5-8(b) and 5-8(c)) had mirror-like surfaces, as shown in Figs. 5-9(b) and 5-9(c), although some surface pits are visible in Fig. 5-9(b). The lattice polarity of the top surface of the freestanding AlN substrates shown in Fig. 5-8 was determined by soaking in KOH solution [42] to be Al-polarity. The FWHMs of the XRD rocking curves for symmetric (0002) AlN and asymmetric $(10\bar{1}0)$ AlN obtained from freestanding AlN substrates were 89.2 and 126.1 arcmin (Fig. 5-8(a)), 38.2 and 24.9 arcmin (Fig. 5-8(b)), and 33.9 and 18.4 arcmin (Fig. 5-8(c)), respectively. Therefore, the crystalline quality of the freestanding AlN substrate was optimum when a 200 nm thick intermediate AlN layer was used. These

results indicate that optimization of the intermediate AlN layer thickness is necessary for the preparation of high quality freestanding AlN substrates, although a thick intermediate AlN layer requires high temperature and long-time heat treatment for the formation of voids.

The optical transmittance of the self-separated freestanding AlN substrates shown in Fig. 5-8 was also investigated. Fig. 5-10 shows transmission spectra of freestanding AlN substrates which was measured at RT in air using UV-visible-near infrared (NIR) double-beam spectrophotometer with normal incidence to the AlN substrates. All of the freestanding AlN substrates were transparent over a wide range of wavelength without evident absorption peaks in each spectrum. The optical transparency disappeared at 208.1 nm (5.96 eV) in all spectra. Photoluminescence (PL) spectra (not shown) of the freestanding AlN substrates shown in Fig. 5-8 were measured at RT using an ArF excimer laser (λ = 193 nm) and also showed peaks at 209.3 nm (5.92 eV). These results show that the obtained freestanding AlN substrates have a wide bandgap of around 6 eV. Meanwhile, the transmittance values of each freestanding AlN substrate were different. For instance, the value of transmittance at a wavelength of 400 nm was 2.8% in Fig. 5-10(a), 30.7% in Fig. 5-10(b), and 56.2% in Fig. 5-10(c). It has been reported that the refractive index of AlN at 400 nm is 2.13 [55]. It is possible to estimate the ideal value of transmittance at a wavelength of 400 nm with this value to be 77%. Therefore, scattering that is caused by the roughness on the top and bottom surfaces of the freestanding AlN substrates is the reason for the smaller measured transmittance values than the ideal value. Moreover, secondary ion mass spectrometry (SIMS) measurements revealed that the impurity concentrations of Si, O, and H in the freestanding AlN substrates shown in Figs. 5-8(b) and 5-8(c) were the same: [Si] = 2×10^{17} cm^{-3}, [O] = 9×10^{18} cm^{-3}, and [H] = 2×10^{18} cm^{-3}. The concentration of O in the freestanding AlN substrate, which is still high, is

likely to decrease by homoepitaxial growth of AlN on the freestanding AlN substrate, because O is thought to be supplied as the sapphire substrate decomposes.

Lastly, TEM observations of the freestanding AlN substrates were performed to evaluate the dislocation density. Fig. 5-11 shows a plan view bright-field TEM image of the top surface of the freestanding AlN substrate shown in Fig. 5-8(c). Dislocations were distributed at random and were linear. This linear appearance of the dislocations indicates that they are inclined from the [0001] direction, because of the high growth temperature of 1450 ºC. Furthermore, the dislocation density of the freestanding AlN substrate was estimated to be 1.5×10^8 cm^{-2}. On the other hand, the dislocation density of the freestanding AlN substrate shown in Fig. 5-8(b) was 1.1×10^9 cm^{-2} [37]. Therefore, the self-separation of a thick AlN layer from a sapphire substrate could prepare a high-quality freestanding AlN substrate with lower dislocation density with a 200 nm thick intermediate AlN layer with voids beneath the intermediate AlN layer.

5.3. Conclusions

Void formation under thin intermediate AlN layers grown by HVPE on sapphire substrates was investigated for the formation of predefined self-separation points of thick HVPE AlN layers. Heat treatment at above 1400 ºC formed voids beneath the 50–200 nm thick AlN layer in mixed carrier gas with added NH_3, because the sapphire decomposed in reaction to hydrogen. Void formation was limited by the diffusion of gaseous Al and/or H_2O through the dislocations in the intermediate AlN layer, and it depended on the heat treatment temperature and time, and the thickness of the intermediate AlN layer. Self-separation of thick AlN layers, which was subsequently grown at 1450 ºC after void formation, took place during post-growth cooling to RT via interfacial voids when an

intermediate AlN layer was 100 nm or more. A freestanding AlN substrate self-separated from the sapphire substrate with 200 nm thick intermediate AlN layer with R_v of 38.0% showed a mirror-like surface, high optical transparency at wavelengths above 208.1 nm, and a low dislocation density of 1.5×10^8 cm^{-2}.

Figures

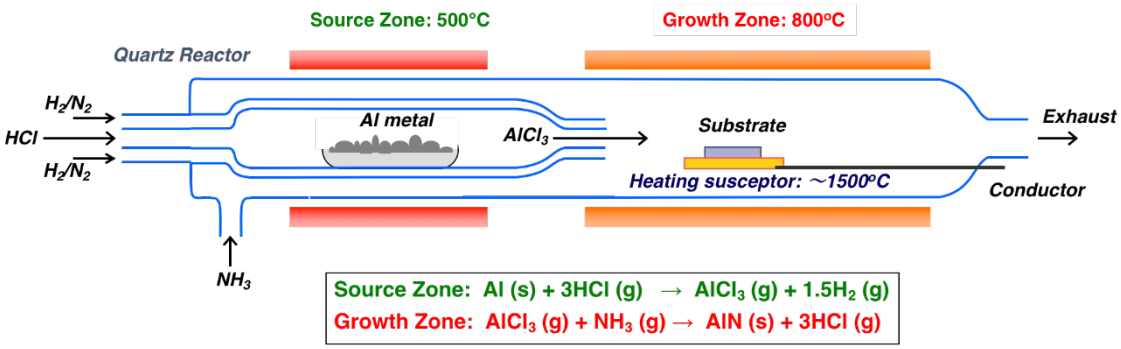

Fig. 5-1. Schematic diagram of the homebuilt HVPE system.

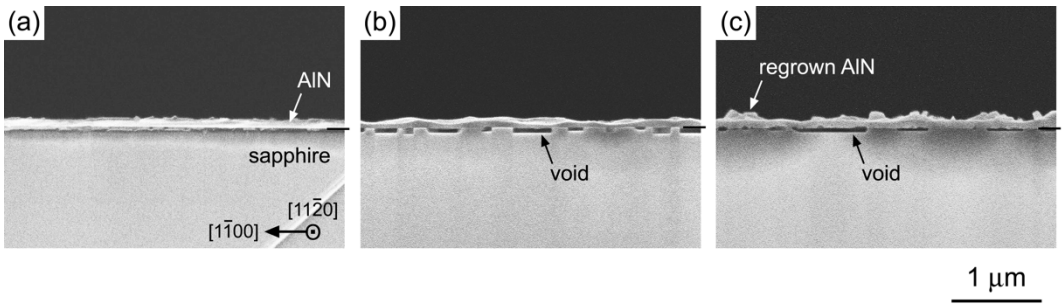

Fig. 5-2. Cross-sectional SEM micrographs of 100 nm thick AlN/sapphire interfaces observed along the [11$\bar{2}$0] sapphire direction after 30 min heat treatment at 1450 ºC in various gas flows: (a) N_2 carrier gas, (b) H_2/N_2 mixed carrier gas with added NH_3, and (c) N_2 carrier gas with added NH_3. Short horizontal lines indicate the interface between the AlN layer and the sapphire substrate.

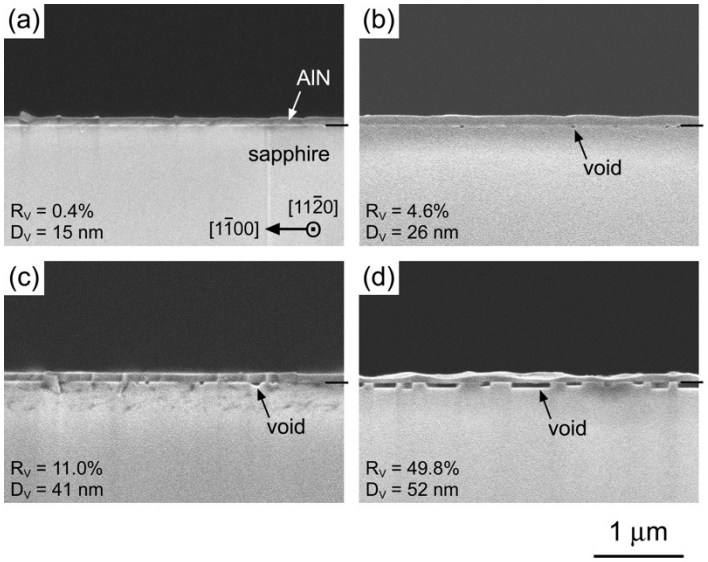

Fig. 5-3. Cross-sectional SEM micrographs of 100 nm thick AlN/sapphire interfaces observed along the [11$\bar{2}$0] sapphire direction after 30 min heat treatment in the H_2/N_2 mixed carrier gas with added NH_3 at (a) 1300, (b) 1350, (c) 1400, and (d) 1450 ºC. Short horizontal lines indicate the interface between the AlN layer and the sapphire substrate.

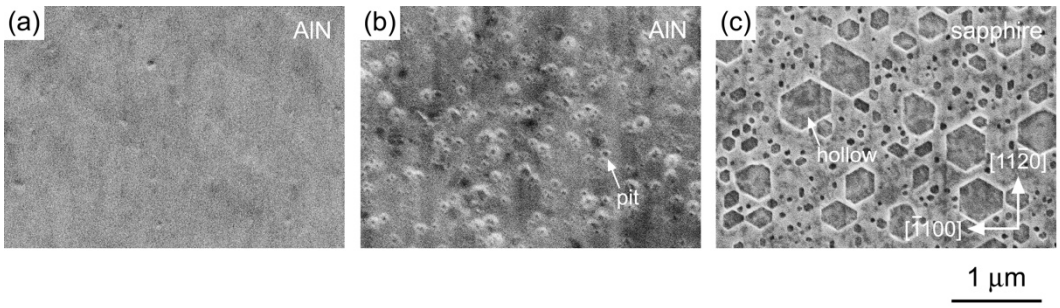

Fig. 5-4. Surface SEM micrographs of a 100 nm thick AlN/sapphire sample heat-treated in the H_2/N_2 mixed carrier gas with added NH_3 at 1450 ºC for 30 min and then observed during etching in KOH solution: (a) just after the heat treatment, (b) after 2 min etching showing pits on the AlN surface, and (c) after complete removal of the AlN layer by etching for 10 min, which revealed a sapphire surface with hollows. Etching was performed using a 5 mol/L KOH solution at 60 ºC.

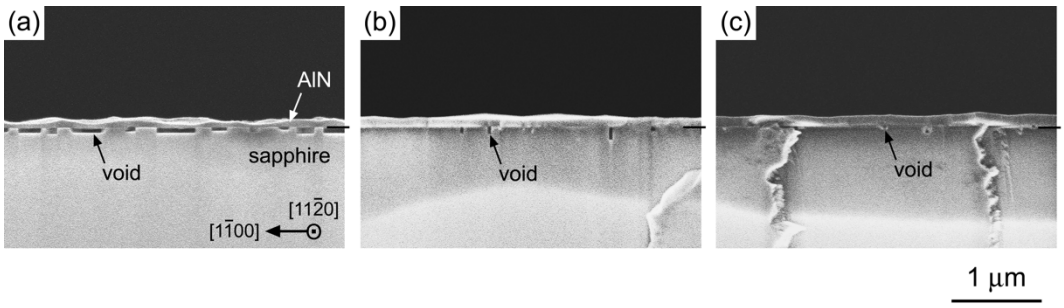

Fig. 5-5. Cross-sectional SEM micrographs of 100 nm thick AlN/sapphire interfaces observed along the [11$\bar{2}$0] sapphire direction after 30 min heat treatment at 1450 ºC in the H_2/N_2 mixed carrier gas with added NH_3. The source gas supply sequence for the growth of AlN layer was (a) $AlCl_3$ preflow for 2 min, (b) simultaneous supply of $AlCl_3$ and NH_3, and (c) NH_3 preflow for 2 min.

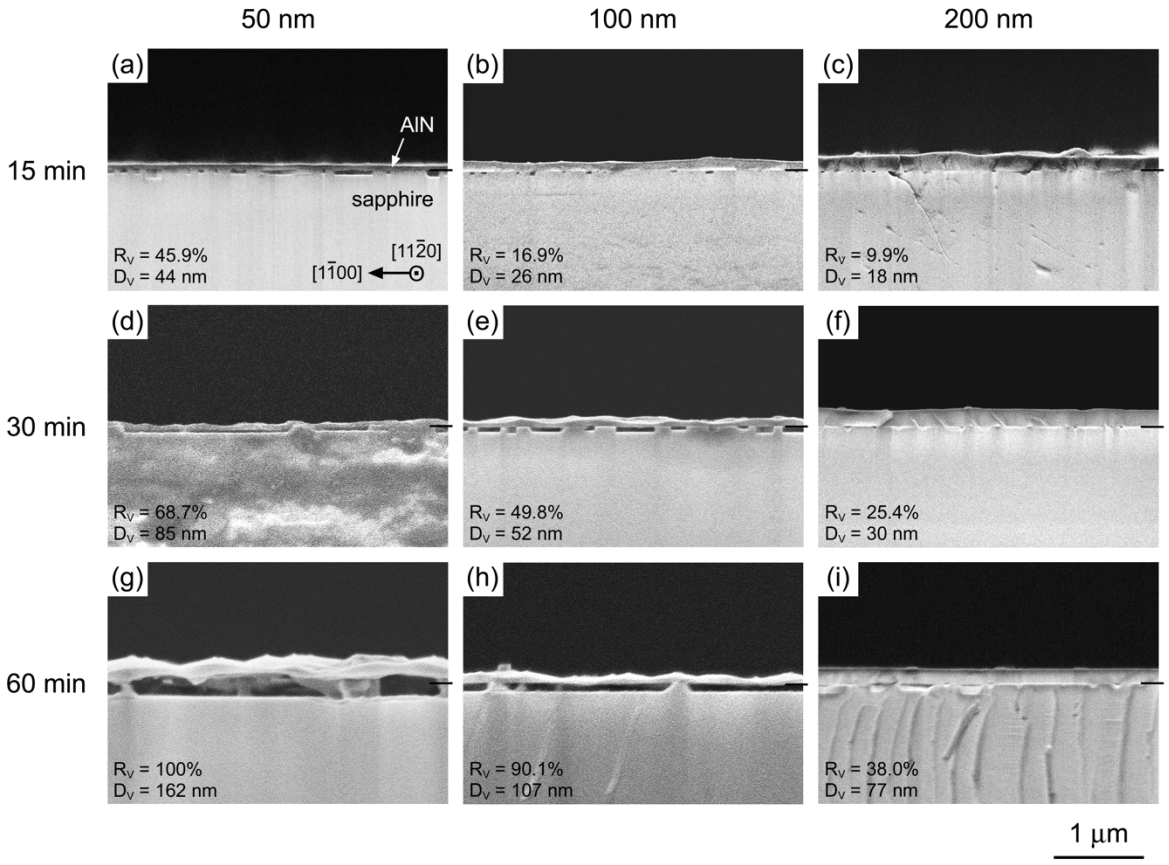

Fig. 5-6. Cross-sectional SEM micrographs of AlN/sapphire interfaces with AlN thicknesses between 50 and 200 nm observed along the [11$\bar{2}$0] sapphire direction after 15–60 min heat treatment at 1450 ºC in the H_2/N_2 mixed carrier gas with added NH_3. Short horizontal lines indicate the interface between the AlN layer and the sapphire substrate.

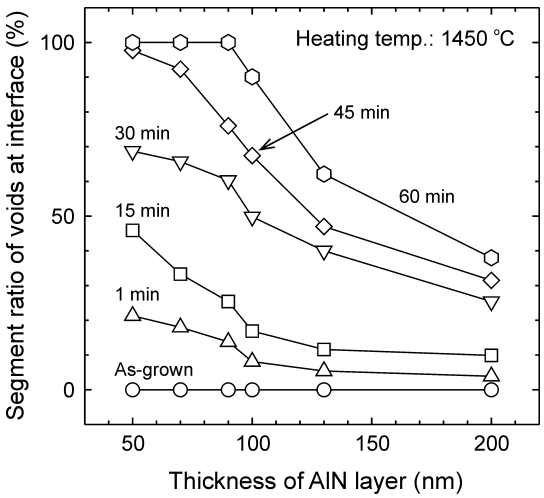

Fig. 5-7. Dependence of the segment ratio of voids at the interface R_v, on the thickness of the intermediate AlN layer and on heat treatment time at 1450 ºC in the H_2/N_2 mixed carrier gas with added NH_3. The R_v value for the as-grown intermediate AlN layer is shown for comparison.

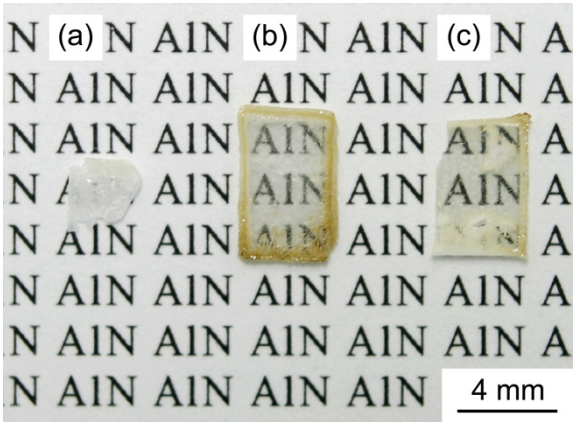

Fig. 5-8. Photograph of freestanding (0001) AlN substrates (79 μm) self-separated from sapphire substrates. The thicknesses of the intermediate AlN layer and the R_v values were (a) 50 nm and 45.9%, (b) 100 nm and 49.8%, and (c) 200 nm and 38.0%, respectively. Void formation beneath intermediate AlN layer was performed at 1450 ºC.

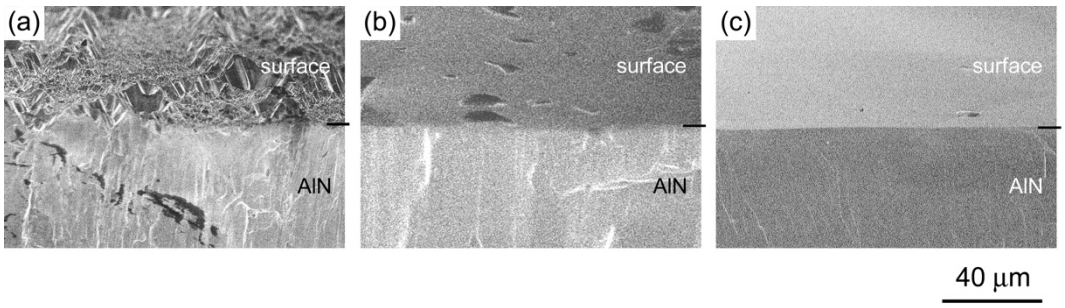

Fig. 5-9. Bird's-eye view SEM micrographs of freestanding AlN substrates self-separated from sapphire substrates. The thicknesses of the intermediate AlN layer and the R_v values were (a) 50 nm and 45.9%, (b) 100 nm and 49.8%, and (c) 200 nm and 38.0%, respectively. Short horizontal lines indicate the boundary of the (0001) surface and ($10\bar{1}0$) cleaved plane.

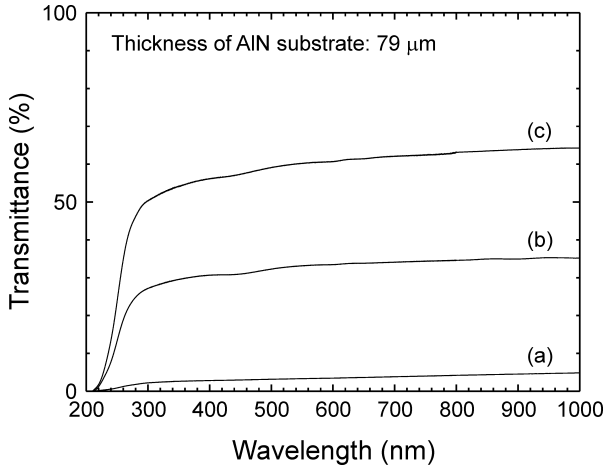

Fig. 5-10. Optical transmission spectra of freestanding AlN substrates self-separated from sapphire substrates measured at RT in air. The thicknesses of the intermediate AlN layer and the R_v values were (a) 50 nm and 45.9%, (b) 100 nm and 49.8%, and (c) 200 nm and 38.0%, respectively.

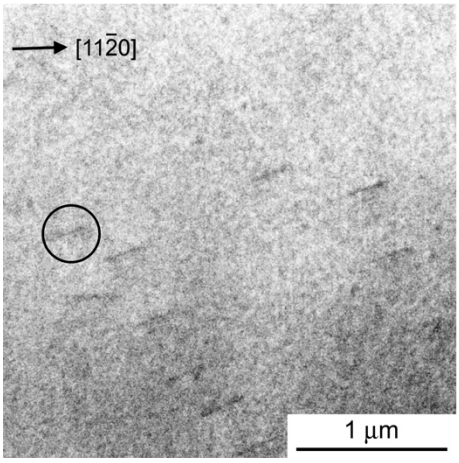

Fig. 5-11. Plan view bright-field TEM image of the top surface of a freestanding AlN substrate at the exact [0001] zone axis of AlN. The AlN substrate was self-separated from the sapphire substrate using a 200 nm thick intermediate AlN layer with R_v of 38.0%. One dislocation is indicated by a circle.

Chapter 6. Summary

In Chapter 2, the thermal stabilities of Al- and N-polarity AlN layers grown on (0001) sapphire substrates were discussed with the investigation at temperatures which ranged from 1100 to 1400 °C in various gas flows (He, H_2 and $H_2 + NH_3$). AlN decomposed in flowing H_2, while it did not decompose in He or $H_2 + NH_3$ flow. The decomposition rate in H_2 increased as the temperature went up over 1200 °C, and the decomposition rate of the Al-polarity AlN layer was lower than that of the N-polarity AlN layer at each temperature. The decomposition reaction of AlN and the relationship between the polarities of the AlN layers and their different decomposition rates were also discussed.

In Chapter 3, the investigation of heat treatment of (0001) sapphire substrates in the temperature range 980–1480 °C was discussed in an atmospheric-pressure mixed flow of H_2 and N_2 for various molar fractions of H_2 ($F° = H_2 / (H_2 + N_2)$). At 1330 °C, AlN whiskers formed on the sapphire surfaces only when the heat treatment was performed when both H_2 and N2 existed ($0 < F° < 1$). The amount of formed AlN was a maximum for $F° = 0.750$, whereas no AlN appeared at $F° = 0$ (N_2 flow) or 1.000 (H_2 flow). When $F° = 0.750$, AlN whiskers formed in the temperature which ranged from 1030–1430 °C, while no AlN formed outside this temperature range. These experimental results are explained by thermodynamic analysis.

In Chapter 4, the formation mechanism of AlN whiskers on (0001) sapphire substrates during heat treatment in an atmospheric-pressure mixed flow of H_2 and N_2 was investigated in the temperature ranging from 980–1380 °C. AlN whiskers grew above 1030 °C after sapphire surface was covered with a thin AlN layer. Existence of pits on sapphire surface beneath the thin AlN layer was discovered. Both densities of the AlN

whiskers and pits of samples heat-treated at 1130 °C were in the same order of 10^8 cm^{-2}. These results lead to the following mechanism. Firstly, sapphire surface reacts with H_2, and generated Al gas reacts with N_2 and thin AlN layer appears on sapphire. After that, sapphire surface reacts with H_2 diffusing to AlN/sapphire interface, and Al gas escapes via dislocations in the AlN layer and leaves pits on sapphire surface. Finally, Al gas immediately reacts with N_2 and forms AlN whiskers at the top surface.

In Chapter 5, the void formation at the interface between thick AlN layers and (0001) sapphire substrates was investigated in order to form a predefined separation point of the thick AlN layers for the preparation of freestanding AlN substrates by hydride vapor phase epitaxy (HVPE). By heating 50–200 nm thick intermediate AlN layers above 1400 °C in a gas flow where H_2 and NH_3 were contained, voids formed below the AlN layers by the decomposition reaction of sapphire with hydrogen diffusing to the interface. The volume of the sapphire decomposed at the interface increased as the temperature went up and time of the heat treatment increased and as the thickness of the AlN layer decreased. Thick AlN layers subsequently grew at 1450 °C after formation of voids beneath the intermediate AlN layer with a thickness of 100 nm or above self-separated from the sapphire substrates while post-growth cooling with the aid of voids. The 79 μm thick freestanding AlN substrate was obtained by using a 200 nm thick intermediate AlN layer, and this had a flat surface with no pits, high optical transparency at wavelengths above 208.1 nm, and a dislocation density of 1.5×10^8 cm^{-2}.

Acknowledgements

I would like to express my special appreciation and thanks to my advisor Prof. Yoshinao Kumagai, who has been a tremendous mentor for me. I would like to thank him for encouraging my research and for giving me priceless experience in my life.

I am deeply grateful to Prof. Akinori Koukitu who has supported industry-academic collaborative research between Tokyo University of Agriculture and Technology and Tokuyama Corporation for many years before I entered the doctoral course.

I would also like to thank my committee members, Prof. Katsuhiko Naoi, Prof. Tatsuo Noma, Prof. Kazuyuki Maeda and Prof. Hisashi Murakami of the Department of Applied Chemistry, and Prof. Tomo Ueno of the Department of Electrical and Electronic Engineering of Tokyo University of Agriculture and Technology for their brilliant comments and discussions.

I would especially like to thank Assist. Prof. Rie Togashi, who is now at Sophia University, and all the members of Kumagai Laboratory for their valuable assistance and friendship.

At the end, I would like to express appreciation to my beloved wife Tomoko for her understanding and continuous encouragement.

References

1) Y. Bilenko, A. Lunev, X. Hu, J. Deng, T. M. Katona, J. Zhang, R. Gaska, M. S. Shur, W. Sun, V. Adivarahan, M. Shatalov, and A. Khan, Jpn. J. Appl. Phys. **44**, L98 (2005).
2) Y. Taniyasu, M. Kasu, and T. Makimoto, Nature **441**, 325 (2006).
3) A. Khan, K. Balakrishnan, and T. Katona, Nat. Photonics **2**, 77 (2008).
4) H. Hirayama, Y. Tsukada, T. Maeda, and N. Kamata, Appl. Phys. Express **3**, 031002 (2010).
5) J. Grandusky, Y. Cui, S. Gibb, M. Mendrick, and L. Schowalter, Phys. Status Solidi C **7**, 2199 (2010).
6) C. Pernot, M. Kim, S. Fukahori, T. Inazu, T. Fujita, Y. Nagasawa, A. Hirano, M. Ippommatsu, M. Iwaya, S. Kamiyama, I. Akasaki, and H. Amano, Appl. Phys. Express **3**, 061004 (2010).
7) J. R. Grandusky, S. R. Gibb, M. C. Mendrick, and L. J. Schowalter, Appl. Phys. Express **3**, 072103 (2010).
8) J. R. Grandusky, S. R. Gibb, M. C. Mendrick, C. Moe, M. Wraback, and L. J. Schowalter, Appl. Phys. Express **4**, 082101 (2011).
9) T. Kinoshita, K. Hironaka, T. Obata, T. Nagashima, R. Dalmau, R. Schlesser, B. Moody, J. Xie, S. Inoue, Y. Kumagai, A. Koukitu, and Z. Sitar, Appl. Phys. Express **5**, 122101 (2012).
10) T. Kinoshita, T. Obata, T. Nagashima, H. Yanagi, B. Moody, S. Mita, S. Inoue, Y. Kumagai, A. Koukitu, and Z. Sitar, Appl. Phys. Express **6**, 092103 (2013).
11) A. Fujioka, K. Asada, H. Yamada, T. Ohtsuka, T. Ogawa, T. Kosugi, D. Kishikawa, and T. Mukai, Semicond. Sci. Technol. **29**, 084005 (2014).

12) M. Shatalov, W. Sun, R. Jain, A. Lunev, X. Hu, A. Dobrinsky, Y. Bilenko, J. Yang, G. A. Garrett, L. E. Rodak, M. Wraback, M. Shur, and R. Gaska, Semicond. Sci. Technol. **29**, 084007 (2014).

13) H. Hirayama, N. Maeda, S. Fujikawa, S. Toyoda, and N. Kamata, Jpn. J. Appl. Phys. **53-11**0209 (2014).

14) S. Inoue, T. Naoki, T. Kinoshita, T. Obata, and H. Yanagi, Appl. Phys. Lett. **106**, 131104 (2015).

15) J. Xie, S. Mia, R. Dalmau, R. Collazo, A. Rice, J. Tweedie, and Z. Sitar, Phys. Status Solidi C **8**, 2407 (2011).

16) Y. Irokawa, E. A. G. Víllora, and K. Shimamura, Jpn. J. Appl. Phys. **51**, 040206 (2012).

17) T. Kinoshita, T. Nagashima, T. Obata, S. Takashima, R. Yamamoto, R. Togashi, Y. Kumagai, R. Schlesser, R. Collazo, A. Koukitu, and Z. Sitar, Appl. Phys. Express **8**, 061003 (2015).

18) L. J. Schowalter, S. B. Schujman, W. Liu, M. Goorsky, M. C. Wood, J. Grandusky, and F. Shahedipour-Sandvik, Phys. Status Solidi A **203**, 1667 (2006).

19) M. Miyanaga, N. Mizuhara, S. Fujiwara, M. Shimazu, H. Nakahata, and T. Kawase, J. Cryst. Growth **300**, 45 (2007).

20) R. T. Bondokov, S. G. Mueller, K. E. Morgan, G. A. Slack, S. Schujman, M. C. Wood, J. A. Smart, and L. J. Schowalter, J. Cryst. Growth **310**, 4020 (2008).

21) P. Lu, R. Collazo, R. F. Dalmau, G. Durkaya, N. Dietz, B. Raghothamachar, M. Dudley, and Z. Sitar, J. Cryst. Growth **312**, 58 (2009).

22) M. Bickermann, B. M. Epelbaum, O. Filip, P. Heimann, S. Nagata, and A. Winnacker, Phys. Status Solidi C **7**, 21 (2010).

23) Z. G. Herro, D. Zhuang, R. Schlesser, and Z. Sitar, J. Cryst. Growth **312**, 2519 (2010).

24) H. Helava, T. Chemekova, O. Avdeev, E. Mokhov, S. Nagalyuk, Y. Makarov, and M. Ramm, Phys. Status Solidi C **7**, 2115 (2010).

25) C. Hartmann, J. Wollweber, A. Dittmar, K. Irmscher, A. Kwasniewski, F. Langhans, T. Neugut, and M. Bickermann, Jpn. J. Appl. Phys. **52**, 08JA06 (2013).

26) Y. H. Liu, T. Tanabe, H. Miyake, K. Hiramatsu, T. Shibata, M. Tanaka, and Y. Masa, Jpn. J. Appl. Phys. **44**, L505 (2005).

27) Y. Kumagai, T. Yamane, and A. Koukitu, J. Cryst. Growth **281**, 62 (2005).

28) O. Kovalenkov, V. Soukhoveev, V. Ivantsov, A. Usikov, and V. Dmitriev, J. Cryst. Growth **281**, 87 (2005).

29) D. S. Kamber, Y. Wu, B. A. Haskell, S. Newman, S. P. DenBaars, J. S. Speck, and S. Nakamura, J. Cryst. Growth **297**, 321 (2006).

30) A. Claudel, E. Blanquet, D. Chaussende, M. Audier, D. Pique, and M. Pons, J. Cryst. Growth **311**, 3371 (2009).

31) Y. Kumagai, Y. Enatsu, M. Ishizuki, Y. Kubota, J. Tajima, T. Nagashima, H. Murakami, K. Takada, and A. Koukitu, J. Cryst. Growth **312**, 2530 (2010).

32) T. Baker, A. Mayo, Z. Veisi, P. Lu, and J. Schmitt, J. Cryst. Growth **403**, 29 (2014).

33) Y. Kumagai, Y. Kubota, T. Nagashima, T. Kinoshita, R. Dalmau, R. Schlesser, B. Moody, J. Xie, H. Murakami, A. Koukitu, and Z. Sitar, Appl. Phys. Express **5**, 055504 (2012).

34) T. Nagashima, Y. Kubota, T. Kinoshita, Y. Kumagai, J. Xie, R. Collazo, H. Murakami, H. Okamoto, A. Koukitu, and Z. Sitar, Appl. Phys. Express **5**, 125501 (2012).

35) T. Nagashima, M. Harada, H. Yanagi, Y. Kumagai, A. Koukitu, K. Takada, J. Cryst. Growth **300**, 42 (2007).

36) Y. Kumagai, T. Yamane, T. Miyaji, H. Murakami, Y. Kangawa, A. Koukitu, Phys. Status Solidi C **0**, 2498, (2003).

37) Y. Kumagai, J. Tajima, M. Ishizuki, T. Nagashima, H. Murakami, K. Takada, A. Koukitu, Appl. Phys. Express **1**, 045003 (2008).

38) Y. Kumagai, K. Takemoto, J. Kikuchi, T. Hasegawa, H. Murakami, A. Koukitu, Phys. Status Solidi B **243**, 1431 (2006).

39) J. Tajima, Y. Kubota, R. Togashi, H. Murakami, Y. Kumagai, A. Koukitu, Phys. Status Solidi C **5**, 1515 (2008).

40) T. Yoshida, Y. Oshima, T. Eri, K. Ikeda, S. Yamamoto, K. Watanabe, M. Shibata, T. Mishima, J. Cryst. Growth **310**, 5 (2008).

41) M. Takeuchi, H. Shimizu, R. Kajitani, K. Kawasaki, Y. Kumagai, A. Koukitu, Y. Aoyagi, J. Cryst. Growth **298**, 336 (2007).

42) D. Zhuang, J. H. Edgar, L. Liu, B. Liu, L. Walker, MRS Internet J. Nitride Semicond. Res. **7**, 4 (2002).

43) D. D. Koleske, A. E. Wickenden, R. L. Henry, M. E. Twigg, J. C. Culbertson, R. J. Gorman, Appl. Phys. Lett. **73**, 2018 (1998).

44) M. Mayumi, F. Satoh, Y. Kumagai, K. Takemoto, A. Koukitu, J. Cryst. Growth **237-239**, 1143 (2002).

45) P. Gay, P. B. Hirsch, A. Kelly, Acta Metall. **1**, 315 (1953).

46) Z. Y. Fan, N. Newman, Mater. Sci. Eng. B **87**, 244 (2001).

47) C. B. Vartuli, S. J. Pearton, J. W. Lee, C. R. Abernathy, J. D. Mackenzie, J. C. Zolper, R. J. Shul, and F. Ren, J. Electrochem. Soc. **143**, 3681 (1996).

48) K. Akiyama, H. Murakami, Y. Kumagai, A. Koukitu, Jpn. J. Appl. Phys. **47**, 3434 (2008).

49) M.W. Chase Jr. (Ed.), NIST-JANAF Thermochemical Tables, Fourth Ed., The American Chemical Society and the American Institute of Physics for the National Institute of Standards and Technology, Gaithersburg, MD (1998).

50) Y. Kumagai, K. Akiyama, R. Togashi, H. Murakami, M. Takeuchi, T. Kinoshita, K. Takada, Y. Aoyagi, A. Koukitu, J. Cryst. Growth **305**, 366 (2007).

51) G. R. Yazdi, M. Beckers, F. Giuliani, M. Syväjärvi, L. Hultman, R. Yakimova, Appl. Phys. Lett. **94**, 082109 (2009).

52) K. Uchida, A. Watanabe, F. Yano, M. Kouguchi, T. Tanaka, S. Minagawa, J. Appl. Phys. **79**, 3487 (1996).

53) H. Fukuyama, S. Kusunoki, A. Hakomori, K. Hiraga, J. Appl. Phys. **100**, 024905 (2006).

54) J. Tajima, Y. Kubota, M. Ishizuki, T. Nagashima, R. Togashi, H. Murakami, Y. Kumagai, K. Takada, A. Koukitu, Phys. Status Solidi C **6**, S447 (2009).

55) H. Takikawa, K. Kimura, R. Miyano, T. Sakakibara, A. Bendavid, P. J. Martin, A. Matsumuro, K. Tsutsumi, Thin Solid Films **386**, 276 (2001).

List of papers related to this research

Chapter 2

"Polarity dependence of AlN {0001} decomposition in flowing H_2"

Yoshinao Kumagai, Kazuhiro Akiyama, Rie Togashi, Hisashi Murakami, Misaichi Takeuchic, Toru Kinoshita, Kazuya Takada, Yoshinobu Aoyagi, Akinori Koukitu

J. Cryst. Growth **305**, pp. 366-371 (2007).

Chapter 3

"Formation of AlN on sapphire surfaces by high-temperature heating in a mixed flow of H_2 and N_2",

Yoshinao Kumagai, Takahiro Igi, Masanari Ishizuki, Rie Togashi, Hisashi Murakami, Kazuya Takada, Akinori Koukitu,

J. Cryst. Growth **350**, pp. 60-65 (2012).

Chapter 4

"Formation mechanism of AlN whiskers on sapphire surfaces heat-treated in a mixed flow of H_2 and N_2",

Kazuya Takada, Kazushiro Nomura, Rie Togashi, Hisashi Murakami, Akinori Koukitu, and Yoshinao Kumagai,

Jpn. J. Appl. Phys. **55**, No. 5S, pp. 05FF01 1-4 (2016).

Chapter 5

"Investigation of void formation beneath thin AlN layers by decomposition of sapphire substrates for self-separation of thick AlN layers grown by HVPE",

Yoshinao Kumagai, Yuuki Enatsu, Masanari Ishizuki, Yuki Kubota, Jumpei Tajima, Toru Nagashima, Hisashi Murakami, Kazuya Takada, Akinori Koukitu,

J. Cryst. Growth **312**, pp. 2530-2536 (2010).

List of international conference presentations

1) “Analysis of formation mechanism of AlN whiskers on sapphire surfaces at elevated temperature in a mixed flow of H_2 and N_2”,

   Kazuya Takada, Kazushiro Nomura, Rie Togashi, Hisashi Murakami, Akinori Koukitu, and Yoshinao Kumagai,

   Sixth International Symposium on Growth of III-Nitrides (ISGN-6), Hamamatsu, Japan, We-A40 (2015).